H4-SMR 471/02

COLLEGE ON MEDICAL PHYSICS

10 - 28 SEPTEMBER 1990

Computed Tomography: Physical Principles
Significant Parameters, Instrumentation

COMPUTED TOMOGRAPHY: PHYSICAL PRINCIPLES,SIGNIFICANT PARAME-
TERS, INSTRUMENTATION.

ROBERTO   CESAREO,   Centro   per   l'Ingegneria   Biomedica   e
Dipartimento   di   Energetica,Universita'   di   Roma   "La
Sapienza",Corso Vittorio Emanuele II,244,00186 Roma,Italy.

Roberto Cesareo

Universita di Roma
Roma
Italy

1

1. Introduction

In a computed tomography (CT) scanner, a number of profiles of narrow-beam transmission are made at different orientations around a subject. From these measurements a reconstruction of a cross section is created.

When a beam of monoenergetic X or gamma-rays crosses a sample, like in tomographic measurements, part of the radiation is absorbed by the sample, part is diffused (elastically or inelastically) and part is transmitted (Figure 1).

The study of the scattered or of the transmitted radiation allows to deduce information on the composition of the crossed volume, and particularly of the physical density, the electron density and of the mean atomic number distribution respectively.

The transmission tomography is based on the study of the radiation transmitted through a sample, and other form of tomographic images are based on the study of the scattered radiation (Compton and Rayleigh tomography) or of the XRF radiation emitted by the irradiated sample volume (XRF-tomography).

A detailed study of the interaction mechanism between radiation and matter is therefore important for understanding the physical basis of all kind of tomographic images obtained by using X or gamma ray sources.

Since the fundamental measurement on which a computed tomography is based is a measurement of narrow-beam X-ray attenuation profiles, it is important to connect the quantitative values from CT-scanners with the average total linear attenuation coefficient.

In Section 2 is discussed the main mathematical-physical problem of CT image: to use the knowledge of the attenuation coefficient sums derived from X-ray intensity measurements made at all the various irradiation directions to calculate the attenuation coefficient of each individual voxel that is part of the CT image.

Photons interaction with matter (photoelectric effect, Compton effect, elastic scattering and pair production), mass and linear attenuation coefficients and its correlation with density and atomic number of the absorbing matter are described in Section 3.

In Section 4 is described the characterisation of human tissues and organs for X-ray imaging, described by its mean composition, density, electron density and attenuation coefficients.

A short history of X-ray tomography and its mathematical basis is presented in Section 5. A qualitative description of mathematical reconstruction methods is given in Section 6, and a description of the main components of a CT-scanner (sources, detectors, mechanics, computers and so on) is given in Section 7.

The various generations of medical CT-scanners are described in Section 8, and the CT-scanners for industrial applications are described in Section 9.

The significant parameters which determine the quality of a CT-image (resolution, artifacts, statistics and so on) are described in Section 10, and in Section 11 are shown several recent imaging techniques based on the analysis of scattered or fluorescent radiation.

2. The problem

In computed tomography,X or gamma rays from a finely collimated source are directed at a slice of the object or patient from variety of directions.

The basic problem in computed tomography is to determine what the attenuation characteristics are for each small volume of object or tissue in the patient slice which would cause the transmitted radiation intensity to be what is recorded for all the various radiation irradiations directions (Figure 2).It is these calculated tissue attenuation,defined with the so called "attenuation coefficient" that actually characterizes the CT-images.

For a monochromatic X or gamma ray beam,the tissue attenuation characteristics can be described by (for more details see Section 3):

$$N = N_o \, e^{-\mu x} \tag{1}$$

where N_o is the incident intensity and N the transmitted intensity through a thickness x of object or tissue with a characteristic attenuation coefficient μ . If a slab of heterogeneous material is irradiated and we divide up the slab into volume elements,or voxels,then let us assume each voxel has its own attenuation coefficient ,where the subscript stands for the j-th voxel,as indicated in Figure 2.

The radiation incident on the first voxel of width Δx is attenuated according to Eq.(1) by a factor $exp(-\mu_1\Delta x)$.The transmitted radiation from the first voxel N_1 ,then becomes the incident radiation to the second voxel N_2 ,which further reduces the intensity of the beam by an attenuation factor $exp(-\mu_2\Delta x)$.Each successive j-th voxel traversed attenuates the beam further by its characteristic attenuation factor $exp(-\mu_j\Delta x)$ until the final beam transmitted from the patient is measured by external detectors. The arithmetic sum $\sum$ of the attenuation coefficients μ_T of all j voxels of width Δx traversed by a given beam of photons is directly related to the ratio of transmitted and incident intensities N_o/N:

$$\frac{N}{N_o} = exp\left\{-\left[\left(\sum_J \mu_J\right)\Delta x\right]\right\} \tag{2}$$

By rewriting Eq.(2) in a slightly different form:

$$\sum_J \mu_J = \frac{1}{\Delta x} \, \ln\left(N_o/N\right) \tag{3}$$

it can be seen that the sum of the voxel attenuation coefficients for each X-ray beam direction can be determined from the experimentally measured beam intensities for a given voxel width.It is the goal in computed tomography to use the knowledge of the attenuation coefficient sums derived from X-ray intensity measurements made at all the various irradiation directions to calculate the attenuation coefficients of each individual voxel that is part of the CT image.

3. X and gamma ray attenuation in matter

Although a large number of possible interaction mechanisms are known, when monoenergetic X or gamma-rays are attenuated in matter, only four major effects are important: photoelectric effect,inelastic or Compton effect, elastic or Rayleigh scattering and pair production (with a threshold energy of 1022 keV).

3a. Photoelectric effect

The photoelectric effect is a two step event in which an electron from a inner atomic shell (K,L,M...) is removed by an incident photon and subsequently an X-ray or an Auger electron are emitted (depending on the fluorescence yield)(Figure 3):

From the conservation of the energy:

$$E_o = E_L + E_{kin} \tag{4}$$

in which:

E_o represents the energy of the incident photon;
E_L represents the binding energy of the electron and
E_{kin} represents the kinetic energy of the ejected electron.

Photoelectric interactions usually occur with electrons that are firmly bound to the atom,that is,those with a relatively high binding energy. Photoelectric interactions are most probable when the photon energy is only slightly more than the binding energy.The probability then decreases approximately as E_o .This energy dependence has important consequences when one wishes to analyze a wide range of elements using a single energy photon source.After the electron is ejected,the irradiated atom will emit X rays resulting from the decay of the excited states. Each element emit a characteristic set of X-rays. A sample containing several elements will emit many X-rays of characteristic energies,and the "efficiency" of this process,called X-ray fluorescence,is related to the energy of incident radiation respect to the edges of the elements irradiated and to be analyzed.

The photoelectric effect is,therefore, the basic effect for the X-ray fluorescence analysis (1).Each element deexcites with the emission of K_α and K_β X-rays that are in a fixed intensity

ratio. K_α rays result from the transition of an electron from the L to the K shell; K_β rays result from the transition from the M to the K shell. In a similar manner, when an electron of the L-shell is removed,the atom deexcited by emitting L_α ,L_β and L_γ X-rays.

As the exciting radiation energy is varied we pass through jumps in the probability of photoelectric effect, known as absorption edges.These absorption edges result from electron in different orbitals becoming available for photoelectric absorption.

The cross section for photoelectric effect is proportional to the atomic number Z of the sample as:

in the low energy region $\quad z^4$

in the high energy region $\quad z^5$ (5)

3b. Compton effect

The Compton (or inelastic) scattering takes place between the incident X or gamma radiation of energy E_o and an electron in the scattering material,supposed free. This effect gives rise to an electron of energy E_c and a secondary photon of energy E,scattered through an angle ϑ with respect to its original direction (Figure 4). The energy E_o of the incident photon is shared between the recoil electron and the scattered photon. The energy E_c of the scattered photon as a function of the scattering angle is given by:

$$E_c = E_o/(1+\alpha(1-\cos\vartheta)) \qquad (6)$$

where $\alpha = E/m_o c^2$ is the reduced energy of the incident photons and $m_o c^2 = 511$ keV is the rest mass energy of the electron. The scattering angle can take on values anywhere between 0 and 360 degrees. Figure 5 shows the energy dependence of Compton scattered radiation E_c as a function of the scattering angle for two different incident photon energies. In case the Compton electron is absorbed in the material,there is not much interest from the analytical point of view, while the scattered Compton photon (degraded in energy) can be used to obtain information about the nature of the absorbing material.

The angular distribution for the Compton scattered X or gamma rays can be calculated with the incoherent scattering function modification to the Klein-Nishina formula.

The differential scattering cross section $d\sigma_c$ /$d\Omega$ (in cm^2/sterad electron) as a function of scattering angle and for not-polarized photons is conveniently given in the form:

$$\frac{d\sigma_c}{d\Omega} = \frac{r_o^2}{2}\left[\frac{1}{[1+\alpha(1-\cos\vartheta)]^2}\left[1+\cos^2\vartheta+\frac{\alpha^2(1-\cos\vartheta)^2}{1+\alpha(1-\cos\vartheta)}\right]\right] S(X,Z) \quad \frac{cm^2/\alpha}{sterad} \quad (7)$$

where $r_o = e^2/m_o c^2 = 2.8 \times 10^{-13}$ cm represents the classical electron radius and S(X,Z) represents the "incoherent scattering function", where X=sin ($\vartheta/2$)/λ is the momentum transfer; $\lambda = 12398/E(eV)$.

The incoherent scattering function S(X,Z) represents the probability that an atom be raised to any excited or ionized state as a result of a sudden impulsive action which imparts a recoil momentum X to an atomic electron. The function S(X,Z) versus the momentum transfer, for water or biological materials (Z=7.5) is shown in Figure 6 (2).

The differential cross section,given by Eq.(7), for water at 20 and 40 keV incident energies are shown in Figure 7 and 8, and for silver at 40 keV in Figure 9.

3c. Coherent scattering

Coherent scattering (or Rayleigh) is described in classical terms as the diffraction of an electromagnetic wave by the electric field associated with the electron charge distribution.

Rayleigh scattering is a process by which photons are scattered by bound atomic electrons and in which the atom is neither ionized nor excited. The scattering from different parts of the atomic charge distribution is then "coherent",i.e. there are interference effects;the scattering from an atom with Z electrons is therefore not given by Z times the scattering from a free e-lectron.

As a consequence of Rayleigh scattering the incident photon is scattered at an angle ϑ respect to the initial direction,con-serving the same energy (Figure 10). This process occurs mostly at low energies and for high Z materials, in the same region where electron binding effects influence the Compton scattering cross section. Indeed,if each atomic electron contributes independently to the cross section, the onset of Rayleigh scattering for low momentum transfer would exactly compensate for the reduction of Compton scattering due to binding.

The differential cross section for Thompson elastic scattering of a photon by a free electron is given by:

$$\frac{d\sigma_T}{d\Omega} = \frac{r_e^2}{2}\left(1+\cos^2\vartheta\right) \qquad (8)$$

If the Rayleigh scattering is extended over the Z electrons of individual atoms,the differential cross section is given by:

$$\frac{d\sigma_R}{d\Omega} = \frac{r_o^2}{2}\left(1+\cos^2\vartheta\right)\left[F(x,Z)\right]^2 \quad \frac{cm^2/atom}{sterad} \quad (9)$$

where F(X,Z) is called the "atomic form factor", and X is the momentum transfer,above defined
The atomic form factor versus momentum transfer,for biological samples, is shown in Figure 11 (2).

Differential cross sections for water at 20 and 40 keV incident energies and for silver at 40 keV are shown in Figures 7,8 and 9. Integrated angular distributions of Rayleigh cross section gives rise to a probability which is small respect to photoelectric effect and to Compton effect. On the basis of these considerations, Rayleigh scattering is frequently disregarded in X and gamma ray transport theory and in tomographic calculations. Rayleigh scattering can,however, be of importance in interpreting "narrow beam" attenuation because of the angular spread of coherent scattered radiation (see Figures 7,8 and 9). Rayleigh scattering should be also considered and discussed for the same reason.
A useful simple criterion for judging the angular spread of Rayleigh scattering is:

$$\theta_c = \lambda \, arcsin \left[\frac{0.0133 \; Z^{1/3}}{E} \right]$$ (10)

where θ is the opening half angle of a cone containing at least 75% of the Rayleigh scattered photons (3).

3d. Pair production
During pair production, the incident photon interacts with the field of the nucleus,disappears,and creates an electron (e-) and a positron (e+). Since the rest mass energy of the two particles are 511 keV each,the threshold energy for pair production is 1022 keV. The excess energy of the incident photon is then equally shared by the electron and the positron in the form of kinetic energy.
The positron,being elettrically charged, is slowed down.Further,because it is antimatter,the positron eventually interacts with an electron,in which case both particles annihilate one another. In their place, two photons having 511 keV energy each are then created. These annihilation photons travel at a 180 angle to one another (Figure 12).
Due to the high threshold energy,pair production cannot occur in the field of X-rays,and it is therefore not contributing at all at X-ray radiography or tomography. This effect could anly contribute to gamma ray tomography,when incident radiation of energy larger than 1022 keV is employed.

3e. Total attenuation of radiation in matter
When a narrow beam of monoenergetic photons with energy E_0 and incident photon flux intensity (number of photons/unit time and area) N_0 passes through an omogeneous absorber of thickness x,

(in cm) then the emerging photon intensity will be given by:

$$N = N_0 \; exp(- \mu(\rho,Z,E)x)$$ (11)

where μ (in cm^{-1}) is the linear attenuation coefficient for material of physical density ρ (in g/cm^3) and atomic number Z (Figure 13) (4).

The total linear attenuation coefficient can be decomposed into contributions from each above described mode of photon interaction as:

$$\mu_{tot.} = \mu_{ph.} + \mu_c + \mu_{coh.} + \mu_p$$ (12)

where $\mu_{ph.}, \mu_c, \mu_{col.}$ and μ_p designate photoelectric effect, Compton scattering,Rayleigh scattering and pair production respectively. Altough linear attenuation coefficients are convenient for engineering applications and shielding calculations, they are proportional to the density of the absorber,which depends on the physical state of the material. Since molecular binding energies are smaller than the energies involved in X-ray radiography and tomography,it is a reasonable approximation to assume that the linear attenuation coefficient is directly proportional to the physical density and write:

$$N = N_0 \; exp(-(\mu(Z,E)/\rho)\rho x$$ (13)

where μ/ρ (in cm^2/g) is the "mass attenuation coefficient".If the absorber is a chemical compound or mixture, its mass attenuation coefficient μ/ρ can be approximately evaluated from the coefficients for the constituent elements according to the weighted sum:

$$\mu/\rho = \sum w_i \left(\mu_i/\rho_i \right)$$ (14)

where w_i is the proportion by weight of the i-th constituent the material.
The mass attenuation coefficient of a compound or a mixture can be,therefore,calculated from the mass attenuation coefficient of the components (5). For example,a compound with formula $X_a Y_b$ will have w_i equal to:

$$w_x = aA_x/(aA_x + bA_y)$$
$$w_y = bA_y/aA_x + bA_y)$$ (15)

As an example of the use of Eq. (14)and (15) the computation of mass attenuation coefficient for plexiglas ($C_5H_8O_2$) at E_0= 60 keV will be carried out with the values of total mass attenuation coefficients for the components carbon,hydrogen and oxygen (0.176, 0.326 and 0.191 cm^2/g respectively); that is:

$$\mu/\rho (C_5H_8O_2) = 60/100 \; \mu/\rho (C)+8/100 \; \mu/\rho (H)+32/100 \; \mu/\rho (O)$$

which yields the value μ/ρ = 0.193 cm^2/g, in good accord with the tabulated values of the attenuation coefficients.

3f. Attenuation coefficients versus atomic number and physical density

The total mass attenuation coefficient μ/ρ is also proportional to the total cross section per atom σ_{tot}^a. The relation is:

$$\mu/\rho \; (cm^2/g) = \sigma_{tot}^a \; (cm^2/atom) \cdot (N_A/A)(atoms/g)$$ (16)

where N_A = 6.03 x 10^{23} is Avogadro's number and A is the atomic mass of the absorber (in g).

Since there are Z electrons per atom:

$$\mu/\rho = \sigma_{tot}^e \left(\frac{N_A Z}{A}\right) = \sigma_{tot}^e \; \delta_e$$ (17)

where σ_{tot}^e (cm^2/electron) is the total cross section per electron and the term (N Z/A) represents the electron density (number of electrons per gram).

For all elements except hydrogen, δ_e approximately equals $N_A/2$ = 3 x 10^{23} ,because Z/A = 1/2 (see Table 1). For hydrogen, δ_e is equal to N_A ,and is therefore twice the "normal" value.

This indicates that atomic composition dependence of μ/ρ is uncorrelated to the term δ_e ,and is related to the term σ_{tot}^e. The linear attenuation coefficient μ is,therefore,approximately depending on Z in the physical density term ρ and expressely depending on Z in the term σ_{tot}^e.

In Table 2 are reported the values of the term σ_{tot}^e versus atomic number Z, at energies of 10,60 and 200 keV.

At 10 keV the main contribution is photoelectric,and the dependence of σ_{tot}^e from Z is very strong:

$$\sigma_{tot}^e \propto Z^3$$

At 60 keV,there is a mixture of photoelectric (at high Z) and Compton effects (at low Z) and the dependence of σ_{tot}^e from Z is of the type:

$$\sigma_{tot}^e \propto Z^{0.8} \quad \text{for low Z (Compton region)}$$
$$\sigma_{tot}^e \propto Z^{1.6} \quad \text{for high Z (photoelectric region)} \quad (18)$$

At 200 keV the Compton effect is largely prevailing at low Z values. Between Z=8 and Z=20 σ_{tot}^e is practically constant,indicating a pure Compton effect.

More specifically, the energy and atomic composition dependence of the mass attenuation coefficient μ/ρ in the energy range of interest in CT scanning of the human body is related to the three modes of photon interaction: i) the photoelectric effect ii) the Compton effect and iii) the coherent scattering.

Over the energy range in CT scanning for the usual biological materials, the Compton effect dominates (Figure 14). However, photoelectric and/or coherent scattering can amount to a significant fraction of the total mass attenuation coefficient. The total mass attenuation coefficient can also be decomposed into three contributions:

$$\mu/\rho = \mu_{ph}/\rho + \mu_c/\rho + \mu_{coh}/\rho$$ (19)

or, in terms of cross sections and electron densities:

$$\mu/\rho = \delta_e \left(\sigma_{ph}^e + \sigma_c^e + \sigma_{coh}^e\right)$$ (20)

It should be observed that,at a given energy, σ_c^e is approximately constant versus atomic number Z (Table 3) and the contribution of coherent scattering is lower than 8% of the total contribution. In this hypothesis:

$$\mu/\rho \simeq \delta_e \left(A + B \; Z^\beta\right)$$ (21)

where A, B and β are constant. The value of β is depending on the energy of incident radiation and on the atomic number of the absorber. Values of are typically between 4.2 and 4.8 in the range Z= 6-12 and E =10 - 100 keV.

In Equation (21) are explicitally separated,in the total mass attenuation coefficient term, the contribution of physical density and atomic number.

In the energy region where the Compton effect is prevailing,the linear attenuation coefficient is linearly proportional to the physical density:

$$\mu_{tot} \simeq \mu_c \propto \rho$$ (22)

In the energy region where the photoelectric effect is prevailing,the linear attenuation coefficient is proportional to

the product of the physical density and to a high power of the atomic number:

$$\mu_{tot.} \simeq \mu_{ph.} \propto \rho \, Z^{(3 \div 4)} \qquad (23)$$

Therefore,the mass attenuation coefficient is proportional to the atomic number only:

$$\mu_{tot.}/\rho \propto Z^{(3 \div 4)} \qquad (24)$$

From measurements with monoenergetic radiation in the Compton region it is possible to determine the density of the material,and from successive measurements in the photoelectric region to determine the atomic number distribution. This is valid in the hypothesis that electron density δ_e can be assumed

constant, and coherent scattering can be neglected. This first assumption is not true for materials containing hydrogen,like biological materials. In this hypothesis:

$$\mu/\rho \simeq \delta_e \, A \qquad \text{or} \qquad \mu(cm^{-1}) \simeq \rho \, \delta_e \, A \qquad (25)$$

in the Compton region,and

$$\mu/\rho \simeq \delta_e \, B \, Z^{\rho} \qquad (26)$$

in the photoelectric region.
From a measurement in the Compton region, with monoenergetic radiation,the product of physical density and electron density can be measured,and from a second measurement in the photoelectric region the atomic number can also be determined.

4. X-ray characterization of normal and pathological tissues

The most important property which determine image contrast in computed tomography is the X-ray attenuation . In particular,knowledge of the attenuation properties of normal and pathological human tissues permits more realistic modelling of imaging systems.
Unfortunately,only a small number of tissue characterization studies have been reported for diagnostic X-ray imaging. Some of these,particularly those involving attenuation measurements of brain tissues, were motivated by the advent of CT.
Comprehensive work for breast are that of Hammerstein et al.(6) (normal breast tissue) and Johns and Yaffe (normal and neoplastic breast tissue)(7).Data for mean tissue composition had been pro-

vided by theICRP(8),and measurements of attenuation coefficients of normal tissues and body fluids and of some pathologies had been carried out by Phelps et al.-(9),and by Rao and Gregg (10). Additional work has been reported ,concerning the chemical composition of normal and pathological tissues,from that (see Section 2e) the attenuation coefficient can be calculated according to the weighted sum formula (see Eq. 14).Weight fractions for materials of biological interest are listed in Table 4. Linear attenuation coefficient of biological materials (blood,fat,muscle,pancreas and liver are listed in Table 5 ,at various energy values. It should be pointed out that the difference between the various tissues and between normal and neoplastic tissues is very low.

5. Computed tomography:hystorical developments and mathematical basis
5a. Hystorical development
In 1956 A.M.Cormack, Lecturer in Physics at the University of Cape Town, was required to supervise the use of radioactive iso-

topes at the Groote Schuur Hospital,because the Hospital Physicist resigned.He was asked to spend 1 and 1/2 days a week at the hospital,attending the use of isotopes.In the course of his work he observed the planning of radiotherapy treatment.
A.M.Cormack writes: "a girl would superpose isodose charts and come up with isodose contours which the physician would then examine and adjust,and the process would be repeated until a satisfactory dose-distribution was found. The isodose charts were for homogeneous materials,and it occurred to me that since the human body is quite inhomogeneous these results would be quite distorted by the inhomogeneities. It occurred to me that in order to improve treatment planning one had to know the distribution of the attenuation coefficient of tissues in the body,and that this distribution had to be found by measurements made external to the body. At that time the exponential attenuation of X and gamma rays had been known and used for over sixty years with parallel-sided homogeneous slabs of material.I assumed that the generalization to inhomogeneous materials had been made in those sixty years,but a search of the pertinent literature did not reveal that it had been done,so I was forced to look at the problem ad initio.It was immediately evident that the problem was a mathematical one. If a fine beam of gamma rays of intensity N_0 is incident on the body and the emerging intensity was N, then

the measurable quantity $g=\ln(N_o/N)=\int f ds$, where f is the variable absorption coefficient along the line L (Figure 2).
Hence if f is a function in two dimensions, and g is known for all lines intersecting the body, the question is: can f be determined if g is known? Again a literature search and enquiries of mathematicians provided no information about it. Fourteen years would elapse before I learned that Radon (11) had solved this problem in 1917" (12).
Cormack realized that a cross-sectional matrix of coefficients could be determined if measurements of X-ray transmission were obtained at many angles and projections through the body. To explore the feasibility of the reconstruction approach to visualization of internal anatomy, Cormack assembled a 7 mCi Co-60 source and a Geiger-Muller detector on opposite sides of a platform on which an aluminum and wood specimen was positioned. Data on the transmission of Co-60 gamma rays at 5 mm increments were processed manually to yield the attenuation coefficients of the specimen as a function of radius. These results agreed well with the known composition of the phantom (13).
Experimental apparatus used by Cormack in 1957 is shown in Figure 15 (13,14).
In the late 1960s and early 1970s, a number of other investigators were exploring various approaches to reconstruction tomography as potential imaging techniques or as possible aids to treatment planning in radiation therapy (15,16) The principal breackthrough in reconstruction imaging, however, was the work of Hounsfield, an engineer at the Central Research Laboratories of EMI, in England.
Hounsfield agreed with Cormack that images of the interior of the body could be reconstructed from a number of X-ray transmission measurements obtained tomographically. He assembled a model CT scanner consisting of a Am-241 source and NaI(Tl) detector. The source and detector were positioned on opposite sides of a motorized lathe bed that could undergo both translation and rotation motion. With this device, Hounsfield was able to generate reconstruction data describing nonsymmetrical test objects (17). However, accumulation of the transmission data required nine days. To obtain a more intense source of radiation, so that the time to collect data could be reduced, the radioactive source was replaced by an X-ray tube.
The early prototype of CT-scanner developed by Hounsfield is shown in Figure 16. With this apparatus images were obtained of a variety of biological specimen, including human brain (Figure 17).
The first clinical scanner was installed at the Atkinson Morley's Hospital in Wimbledon (Figure 18).

5b. Mathematical basis for computed tomography
When a narrow beam of monoenergetic X-rays of energy E_o and

intensity N_o crosses a specimen, then the output beam is given by the well known relationship:

$$N = N_o \, e^{-\mu s} \qquad (26)$$

for homogeneous specimen, and:

$$N = N_o \, e^{-\int_L \mu(s)\,ds} \qquad (27)$$

for an inhomogeneous specimen (Figure 19). In Eq. (27), s represents the space coordinate, and L is the thickness of the sample crossed by the radiation. By defining $g_L = \ln(N_o/N)$, Eq.(27) can be written as:

$$g_L = \int_L \mu(s)\,ds \qquad (28)$$

As observed in Section 5a, the main mathematical problem is therefore to determine the distribution of the linear attenuation coefficients $\mu(s)$ through the section of the specimen crossed by the radiation, which is under integral, from the knowledge of the terms g (from each attenuation measurement, by rotating and translating the sample, one obtains a value of g_L (Figure 19).

6. Reconstruction methods
6a. Iterative computation of images
Figure 20 gives a simple illustration of how the image of attenuation coefficients may be obtained iteratively by successive approximations from the knowledge of ray sums derived from the measured intensity data..
Let us consider the section of the object divided into six voxels composed of the attenuation coefficients shown in Figure 20. These values are not known a priori because they represent characteristics of the object within the object itself. What is known by scanning the object with X-rays are the sums of these values along various ray directions.
For scan I the horizontal sums 3.12, 2.72 and 3.2 are obtained; this set of data is distributed along the appropriate raw with equal weighting, i.e. for the first raw 3.12/3=1.04, for the second 2.72/3=0.907 and for the third raw 3.2/3=1.07. The resulting image of the first iteration is shown in the right.
The matrix itself is next summed vertically, and its ray sums of 3.17, 3.17 and 3.17 are compared with the experimental values of 3.02, 3.2 and 2.82 respectively, from object scan II. The difference of 0.15, -0.03 and 0.35 are now distributed with equal weighting vertically so as to cause a diagonal sum of the new image matrix to match the experimental data of the scanned

object.The resulting image of the second iteration is shown in the right.
The resulting matrix is then summed diagonally,giving rise to the values (from left to right) of 1.071, 2.039, 3.013, 1.942 and 0.974, which are compared with the experimental values 1.05, 2.17, 2.85, 1.95, 1.02. After distribution with equal weighting one obtains the third scan, which values are reported in the right of same Figure 20.
6b. Simple back-projection
Suppose that the transmission of X-rays through a spherical object is measured along many rays from two views at right angles to each other.At each view,the measurements constitute a profile of X-ray transmission for a particular angular orientation. X-ray transmission profiles are shown in Figure 21.
After the X-ray transmission profiles have been obtained, the process can be reversed,to forme a crude image of the sphere. The reversal process,known as backprojection,is easily implemented without sophisticated mathematics.
Simple back-projection techniques can be explained in another way.Suppose that a series of X-ray transmission measurements are made at different orientations across a single plane through the cube shown in Figure 22, resulting in the X-ray transmission data noted on the axis, corresponding to 14 measurements along the y axis and 10 measurements along the x axis.
To initiate back-projection, each transmission X-ray is divided into 10 parts and each transmission Y-ray into 14 parts. An area of 10 x 14 pixels is then delimited. Each ray reveals 5,20,50 and 100 percent transmission, corresponding to 95,80,50 and 0 percent attenuation respectively. Each part of the ray is assumed to contribute equally to the absorption. For example the ray transmitted along the x-axis with a value of 5 is attenuated by 95%,and each of the 10 cells in the x-axis contributes per-cent.In Figure 23 these attenuation figures are added along the two axis,giving rise to the numbers shown in Figure 23 B.

7. CT-instrumentation
7a.Radiation sources
All types of radiation sources emitting X or gamma rays,monoenergetic or not,can be used for tomographic imaging.
Optimum energy value is depending on thickness,composition and density of the sample,according to the general rule:

$$\mu x = 1 \div 6 \qquad (29)$$

for an homogeneous sample of thickness x(cm) and linear attenuation coefficient μ (cm^{-1}), and:

$$\sum_i \mu_i \Delta x_i = 1 \div 6 \qquad (30)$$

for heterogeneous samples.
For medical applications the sample is the human body,with composition and attenuation coefficient similar to that of water.For example, for a 30 cm body thickness, the condition (29) can be written as:

$$\mu = 0.03 \div 0.2 \ cm^{-1}$$

corresponding to the optimum energy range:

$$60 \ keV < E_o < 500 \ keV$$

More energetic radiation would be needed when bone is present in the sample.
When possible,the general rule given by Eq.(29) should be applied, giving rise an aptimal energy interval for tomographic measurements.
For medical diagnostic purposes,therefore, one of the most strict restriction is given by the scanning time, which must be limited as much as possible.
For this reason,the only practical source is given,in that case, by a high intensity X-ray tube,in spite of its radiation output,which is given by bremsstrahlung and not by monoenergetic radiation.

X-ray tubes
X-ray tubes will be discussed in details in the notes of G.E.Gigante. Here we only remember that in a X-ray tube, X-rays are produced by the interaction of electrons with matter. In simplistic terms, a beam of electrons directed at a target (anode) is decelerated by forces between the incident electrons and the atomic nuclei of the target material (Figure 24).Since a deceleration implies that kinetic energy is lost,one of the ways in which the electron loses energy is by creating a photon of electromagnetic energy equal in energy to the kinetic energy loss. This process is called bremsstrahlung, and if a large number of electrons interact with a target material, the resulting bremsstrahlung consists of photons with a continuum of energies from zero to a maximum equal to the initial electron kinetic energy. The shape of the spectrum remains the same regardless of the kinetic energy of the electrons (Figure 25). The efficiency of X-ray production by bremsstrahlung is directly proportional to the product of the atomic number (z) of the target material and the kinetic energy of the electrons. Since the portion of kinetic energy of the incident electrons that is not converted to X rays results in heating the target material, it is derirable to increase the efficiency of B.S. production as much as possible by utilizing high-energy electrons and target materials of high z. The best target material, due to its high z,

high melting point, good heat transport and low cost, has been found to be tungsten (W). At energy commonly employed in medical applications, approximately 1% of the kinetic energy of the electrons is converted to B.S. by electrons interacting with a W-target. The remaining 99% of the incident energy results in heating the target.
Electrons impinging on the target material also interact with the orbital electron of the atoms. If the incident electron has a kinetic energy greater than the binding energy of an orbital electron, the bound electron may be ejected from the atom in the same manner as described in Section 2a. Characteristic X-rays of the target are then emitted (Figure 26).
Photon intensity from an X-ray tube is depending on a number of parameters like the tube potential and current, the anode material, the geometry of the tube assembly and so on. At the maximum output conditions, a photon intensity of about 10^{12}-10^{14} photons/s can be obtained.

Monoenergetic radiation from an X-ray tube
Quasi monoenergetic radiation can be obtained from an X-ray tube using external secondary targets (1).
When the primary bremsstrahlung radiation from a tube impinges an external target, it is "converted", through photoelectric effect, to secondary X-rays of the element constituting the target. X-rays are emitted from the target (usually K_α and K_β -lines) and collimated. By varying the material of the secondary target, X-rays can be produced of variable energy. The high voltage of the tube may be modulated as a function of the secondary target.
A typical experimental set-up for producing quasi monoenergetic radiation with an X-ray tube is shown in Figure 27. The primary and secondary radiation are both collimated, and the collimators are internally covered by the same material of the target. The conversion of bremsstrahlung radiation in monoenergetic radiation is relatively high, depending on the distance between tube output and secondary target, on the high voltage of the tube, and on the target material. Due to the fact that radiation coming out from the tube is already focused, and the intrinsic target conversion factor ranges between   and   , the total conversion factor ranges usually between   and   .
Considering the secondary X-rays as emitted isotropically by the target, the main loss in intensity is given by the solid angle defined by the target and the output collimator. Considering all those contributions, a total loss of 10^{-2} - 10^{-3} can be considered normal for a system of the type shown in Figure 27.
The background under the monoenergetic lines is depending on the competitive processes respect to the photoelectric effect, i.e. on the ratio of the scattered to the photoelectric effect. This ratio is increasing with decreasing of the atomic number of the target. Examples are shown in Table 6.

When completely monoenergetic radiation is needed, than the intensity of the K_β -line can be strongly lowered respect to the K_α -line, when an absorber is put, after the output of the secondary collimator, containing an element which discontinuity edge energy lies between the energies of K_α and K_β -lines. If the absorber is a water solution containing the element itself, calculating the thickness of the water solution and the concentration of the element, one can improve the ratio K_α /K_β ad libitum (18). The intensity of the monoenergetic output is unfortunately decreasing with the improving of the K_α /K_β ratio.

Radioisotopes
Radioisotopes, both emitting X or gamma radiation are available and may be used for CT-images.
A suitable radioisotope for CT-images should be characterized by the following properties:
-a relatively long half-life
-the emission of only one or two major lines
-an adequate intensity
-a reasonable price.
In the X-ray range, the principal radioisotopes that can be therefore employed are:
Cd-109, emitting Ag-X lines (22 and 24 keV) having a half-life of 453 days
I-125, emitting Te-X lines (27.4 and 31.3 keV) having a half-life of 60 days
Am-241, emitting a gamma line of 59.6 keV, having a half-life of 433 years
Gd-153, which emits 97 and 103 keV gamma rays, with a half-life of 211 days
I-192, which emits several gamma lines (296,308,316 keV), with a half-life of 74 days
Cs-137, emitting a gamma line of 662 keV, with a half life of 30 years
Co-60, emitting two gamma lines of 1173 and 1332 keV, with a half life of 5.3 years.

Synchrotron radiation
Synchrotron radiation (SR) is generated when electrons with typically several billion electron volts (GeV) of kinetic energy orbit in an ultrahigh vacuum tube between the poles of a strong magnet. A vertical magnetic field deflects the electrons horizontally, causing the emission of SR. The SR spectrum is characterized by the critical photon energy (E_c), which is the energy above and below which one-half of the total emitted SR power falls. E_c and the energy range of the spectrum are dependent on the electron energy (E) and the orbital radius (R):

$$E_c = 2.218 \ E^3/R$$

where E_c is in keV, E is in GeV and R is in meters.
A typical spectrum of SR with the storage ring operating at 3 GeV,compared with a W-targetX-ray tube is shown in Figure 28.
The availability of SR sources provides some advantages in comparison with conventional X-ray tube sources presently used.
The advantages are:
1. high photon flux is available to irradiate the sample (several orders of magnitude greater than for most tube sources); therefore the beam can be monochromatized and,if necessary, highly collimated.A beam of submillimeter dimensions can be obtained
2. the radiation is highly polarized in the plan of the electron orbit,which reduces Rayleigh and Compton scattering by the sample
3. the radiation varies in energy from few keV to about 50 keV in energy.

Collimation of the radiation
As observed above, CT-images are characterized by a source, emitting monoenergetic or bremsstrahlung radiation, a movable sample (the human body in medical applications) and a detector (or more detectors). A large number of attenuation measurements are then carried out,and the distribution of physical density or atomic number in the crossed section is determined,using mathematical procedures, through the measurement of the linear attenuation coefficients. For optimal measurements, the so called "narrow beam" set-up is required, consisting in a strong collimation of the incident and output beam from the sample (Figure 13).
In such a manner,the contribution of scattered photons into the detector is strongly reduced,allowing:
a.the correct determination of the attenuation coefficients
b.the improving of the quality of the images.
The concept of attenuation coefficient measurement is related to the hypothesis that only photons are collected in the detector,which never have interacted with the matter,along its straight way from the source to the detector. From a practical point of view, this condition could never be completely satisfied, because of the small amount of forward coherent scattered radiation.This contribution can only be approximately evaluated, by measuring the value of attenuation coefficients versus the diameter of the collimators, and extrapolating the values of attenuation coefficients to the value of zero for the diameter.
From the point of view of the image,the interactions of source radiation with the sample and other structures in the beam path result in the production of copious quantities of scattered radiation by the Compton and coherent processes.
The portion of this scattered radiation directed toward the detector or any image receptor, will destroy the imaging

geometry, which consists of straight lines from the focal spot to the detector. The intensity of this scattered radiation is proportional to the collimation of the beam.
In general scattered radiation reaching the detector does not contribute to the useful imaging process, but will produce a general background intensity, reduce the contrast and decrease the signal to noise ratio of the image.The production of scattered radiation is reduced by limiting the spatial extent of the X-ray beam by means of devices called collimators.
If,for example, a long cylindrical collimator of internal diameter ϕ is employed,a "pencil" beam is obtained,of cylindrical shape and of same diameter close to the output of the collimator,then conical.
In the hypothesis of a point source of energy E_o and a cylindrical collimator (Figure 29) we can distinguish two extreme possibilities:
a)the contribution from scattered radiation from the wall of the collimator is negligible; the output radiation cone is simply given by the solid angle source-collimator (Figure 29A)
b)a large number of output photons is given by scattered photons from the wall of the collimator; the output radiation cone will be enlarged from this process.
The prevailing of condition a) or b) is depending on penetration of the incident radiation in the collimator walls and in the relative contribution of scattered radiation. Photoelectric effects in the collimators is not a disturbing effect, because of the emission of radiation of lower energy, which can be easily distinguished.Forward Compton effect is at the contrary giving rise to radiation of energy close to E_o ,difficult to discriminate, and Rayleigh effect is giving rise to E_o photons.
Considering brass and lead collimators, the mean penetration versus energy and the intensity of the scattering effects respect to photoelectric are shown in Table 7.
It appears evident, from the analysis of the Table, that the collimation effect at the source is more efficient at low energies, for cylindrical collimators.
An exact calculation of the output beam profile is very difficult,because of the multiple scattering effects at the walls of the collimator. It is in any case important to use collimator material of high atomic number for improving the collimation effect.
A solution for better collimating X-rays is given by two discs of a metal with high atomic number,with a hole of appropriate diameter in the middle, lined with the X-ray beam (Figure 30).
This collimation system needs a careful allignement, but gives rise to less scattered radiation respect to the cylindrical collimator (Figure 30 A and B). The collimation is effective for thickness of the filters much larger than the corresponding x values.

Fan beam geometry
Starting with the second-generation CT scanners,more detectors
were added, and it became increasingly difficult to maintain the
allignment of each pencil X-ray beam... To overcome this
difficulty, a continuous fan of X-rays was substituted for the
pencil-like X-ray beams, no collimation was needed at the source,
and each detector was collimated to accept only X-rays along a
line extending from the X-ray target. The fan-beam geometry
irradiated a greater volume,and more scattered radiation was
produced. The detectors had to be shielded from this scattered
radiation. Also, the detectors had to be balanced carefully so
that they were all equally sensitive to the impinging radiation.
The pencil-beam geometry and the fan beam geometry are
illustrated in Figure 31.
7b. Detectors for CT-imaging
In earlier CT scanners,sodium iodide detectors,operated in
current mode, are used to record the transmission of X-rays
through the patient. These detectors,widely used in physics
research,provide high efficiency for detection of X-rays.
However, NaI detectors have a few disadvantages that have made
their application less desirable in the faster CT scanners :
1)non linear response for radiation of different intensities;
2)a limited dynamic range
3)an afterglow of the NaI crystals that could permit the emitted
light to carry over from one sampling interval to the next.
Two approaches have been taken to overcome the limitations of NaI
detectors. The first is the identification of other scintillation
detectors; the second is the use of ionization chambers or solid
state detectors.

a) scintillation detectors
Two scintillation detectors have been identified as possessing
properties superior to NaI for CT scanners: the first to be tried
was calcium fluoride doped with europium CaF (Eu).
This detector is a tranparent,hard material useful for detecting
X and gamma rays up to several hundred keV. This crystal is less
efficient than NaI, but has the notable characteristic of the
lack of long term light decay following intense excitation
(afterglow). This property is particularly valuable in pulsed X-
ray applications where high intense flux are encountered. The
decay constant of CaF (Eu) is 0.94 μs.
A typical gamma ray spectrum is illustrated in Figure 32.
A second scintillator that has been adopted widely is bismuth
germanate (Bi Ge O ,usually abbreviated as BGO). This crystal
has some attractive properties.It has a high stopping power,due
to its high density and effective atomic number, and therefore
provides an efficiency of almost 100% for X-rays employed in CT-
scanners. Further,it has a short decay constant of about 0.3 s
and a very low afterglow. Figure 33 shows the "full energy peak
efficiency" of a BGO and a NaI detector of same size.

Some recent scanners employ CsI activated with thallium coupled
to silicon photodiodes rather than photomultiplier tubes.They
have high detection efficiency,rugger physical character and
energy resolution close to that of NaI(Tl).
b) Ionization detectors
As an alternative to scintillation detectors xenon-filled
ionization chambers are used in some CT-scanners. To improve the
X-ray detection efficiency of these detectors, thay are operated
under high pressure (8-10 atm). In such a manner,these detectors
have about 60% efficiency in absorbing diagnostic X-rays. Xenon-
filled ionization detectors have proved equal to scintillation
detectors for CT scanning. The lower cost of ionization chambers
is a major advantage over scintillation detectors.
c) Solid-state detectors
Solid-state detectors have never been used in CT-scanner till
now, because its high cost and relatively low efficiency.
In the future,mercuric iodide (HgI) array detectors could be
useful for X-ray detection, particularly when monoenergetic
radiation could be used for CT-images (19).

7c. Hardware and software for CT-image reconstruction
Digital computers are now an integral part of medical imaging. In
some applications,such as CT and MRI, computers are part of the
system. In other applications, such as digital radiography,
ultrasound imaging and industrial CT, special-purpose computers
are built into the equipment. In general the computer performs a
variety of functions as:
-data acquisition
-image reconstruction
-image storage
-image processing
-image analysis

The data acquisition system (DAS)provides an interface between
the nuclear electronics connected to the X-or gamma ray detector
and the central processing unit that recontructs an image.
The DAS accepts electrical signals from the electronics,converts
these signals into a digital format and transmits the signal to
the central processing unit.
The CPU is the section of the data processing system in which all
arithmetic operations occur.The sequence of instructions that
yields a specific result is termed a programme.
In general,the image reconstruction programme is composed by
several parts; the first operation consists in transforming the
transmission measurements numbers into a matrix and then to
reconstruct the image by using 1)simple-back projection methods,
or 2)filtered back-projection methods or 3)iterative methods.
Finally,a matrix is obtained of CT numbers or of attenuation

numbers. The image is structured in an array of individual picture elements, or pixels (or voxels for volume elements). Each pixel or voxel is represented by a numerical value,its attenuation coefficient or a multiple of this like the Hounsfield number or CT number.

The digital image is then stored in the computer memory.

The final phase is the conversion of the digital image into a video display. This phase consists in relating the pixel CT number values to the shades of gray. The image is determined by the window levels selected by the operator. Through the manipulation of the upper and lower window levels, it is possible to adjust the contrast of the displayed image.

Further,the image quality can be improved by processing the image,i.e. by filtration processes. Some of the mathematical filter algorithms used in the reconstruction process can reduce image noise by smoothing the image. Some compromise must be considered in using these filter functions.

8. Medical CT-scanners:Four generations of computed tomographic scanners

8a. First generation CT-scanners

The original first generation CT scanner was the EMI unit installed in 1971 in Wimbledon. The basic features of this scanner are shown in Figure 34 . The X-ray beam is collimated into two parallel pencil-like X-ray beams, which are directed toward two NaI scintillators adjacent to each other on the opposite side of the patient. In this manner,transmission data can be collected simultaneously for two adjacent tomographic images of the patient's head. The X-ray tube,collimator and detectors are part of a common frame that scans across the patient so that the X-ray tube and detectors move in synchrony on opposite side of the patient.

The X-ray transmission measurements are delivered to a computer,which generates a set of equations equal in number to the number of transmission measurements. From these equations,a series of CT numbers is computed to be displayed as a gray scale image on the display unit. In the first CT scanner, the display unit provided an 80 x 80 matrix of 6400 voxels.

8b. Second-generation CT-scanners

The adjacent detectors in the first generation scanner permit simultaneous collection of data for two adjacent tomographic sections. It was then recognized that increased speed could be gained by placing more detectors side by side in the same scan plane (Figure 35). Subsequent developments have led to as many as 52 detectors in the scan plane. As more detectors were added, it became difficult to maintain the allignement of each pencil X-ray beam in the fan-shaped geometry. To overcome this difficulty, a continuous fan of X-rays was substituted for the pencil like X-ray beams,and each detector was collimated to

accept only X-rays along a line extending from the X-ray anode. The fan beam geometry irradiated a greater volume of tissue,more scattered radiation was produced and the detectors had to be shielded from this scattered radiation.

Data collection times for a single tomographic section were reduced to about 5 seconds.Further efforts to reduce scan time led to the third generation of CT scanners.

8c. Third-generation CT-scanners

With second-generation CT scanners,scan times still are limited by the need to move the X-ray tube and detectors through two degrees of motion, translational and rotational. By simplifying the motion solely to rotation such that the X-ray tube and detectors simply rotate around the patient,scan times can be reduced even further (third-generation CT-scanner). Modern versions of these scanners employ over 500 detectors extending over an arc between 21 and 45 degrees on the side of the patient opposite the X-ray tube.A diagram of the third-generation scanner is shown in Figure 36. Data collection times for a single image are reduced down to 2.5 seconds.

8e.Fourth-generation scanners

In the fourth-generation scanner,more than 600 detectors are positioned side by side to form a ring that completely surrounds the patient.These detectors remain stationary while the X-ray tube rotates inside the ring and around the patient's body (Figure 37).With this scanning geometry,data for a single image can be collected in as short a time as 2 seconds.The major disadvantages of these scanners are the high cost associated with the large number of detectors,an increased susceptibility to scattered radiation and unused primary radiation directed toward spaces separating the detectors.The radiation dose to the patient is therefore usually greater.

8f.Fifth-generation CT-scanner

Further reductions in scan time are limited mostly by the output of the X-ray tube.

In the Dynamic Spatial Reconstructor scanner,28 X-ray tubes are positioned around a semicircular gantry.The tubes are in line with 28 light amplifiers and TV cameras. The gantry of X-ray tube is rotating continuously around the patient at 15 revolutions per minute.Data-collection views over 360 degrees are obtained in less than 2 seconds.In this manner,images will be produced for data collection times as short as 16 milliseconds.

9. CT-scanners for non-destructive testing

In the medical field X-ray computed tomography is a method for obtaining cross-sectional images of an object without direct contact.

Recently, these medical CT systems have been applied to non-

destructive inspection of industrial materials. The object materials are,however,limited to low density materials such as plastics,ceramics, and aluminum and its alloy due to the low transmission capability of soft X-rays.
Most medical CT-scanners employ intense X-ray sources from a tube in order to complete the measurements within run times of a few seconds, but the continuous X-ray spectrum gives rise to beam hardening artifacts which degrade the images. In many industrial CT applications the speed of measurements can often be relaxed to some degree and this enables gamma-ray sources to be used instead of an X-ray tube which directly eliminates the beam hardening problem if single photon counting is employed with energy dispersive detectors. Gamma-ray sources also offer additional advantages compared with X-ray tubes,including lower cost,compactness, portability and ready access to a very wide range of photon energies; the constancy of gamma photon energy over space and time also renders gamma tomography a more objective method of imaging.
Therefore for precise quantitative imaging gamma-ray sources are superior to X-ray tubes in almost all respects apart from the question of source brightness; for example the X-ray tube in a medical CT machine can have typically an equivalent strenght of 10000 Ci (more than 10^{14} Bq) distributed over a few millimeters, which is several orders of magnitude brighter than practicable gamma sources. Despite this drawback gamma-ray sources ranging from a few millicuries to 200 Ci have been used to achieve useful tomographic images in acceptable run times. Clearly, optimal photon utilisation is particularly important when using such sources and this is generally obtained, in CT-transmission tomography, by using a fan beam geometry together with multiple detectors (see Section 7a)(20).
Practicable gamma sources cover an energy range between hundreds of keV to about 1.3 Mev of Co-60 (21). That limit the thickness of the metallic object to analyzed to about 5-10 cm.
For larger objects,bremsstrahlung radiation from high-energy X-ray sources can be employed, ,like for example the megaelectron-volt Linatron X-ray sources, which are capable of inspecting objects up to meters in diameter, like missile shroud motors, space propulsion motors ,aircraft structures and so on (22).
Non medical X or gamma rays CT-scanners have been applied to very different fields, like soil physics (23,24)),mechanical engineering (mainly for analysis of motors of all types,turbines,castings)(22,25), building engineering (analysis of costruction materials (26) archaeometry (analysis of statues, columns and so on)(26,27)),nuclear science (measurement of void fraction) (28),metals analysis (homogeneity of alloys, density control,analysis for steel industry ,nozzles)(29).

10. Significant parameters in CT-imaging
10a. CT numbers and Hounsfield numbers
The CT numbers of a CT-unit represents the "effective" linear attenuation coefficients of the various materials being analysed. It corresponds to the linear attenuation coefficient when monoenergetic radiation would be employed, otherwise it is a mean value integrated over the bremsstrahlung spectrum.
In order to be able to differentiate various kinds of body tissues or of various materials, the CT-scanner must be able to measure the effective linear attenuation coefficients correctly for a wide range of materials from air to compact bone in the medical field) or from air to uranium (in non destructive testing). The CT-scanner must be able to detect small differences in the way different substances or materials stop radiation. For medical images, the Hounsfield numbers are used, defined as:

$$ H = 1000 \left(\frac{\mu_x - \mu_w}{\mu_w} \right) \tag{31}$$

in which μ_x represents the attenuation coefficient of a given material and μ_w the water attenuation coefficient at same energy.If x=air, then $\mu_{air} \ll \mu_w$, H=-1000; for x=water, H=0.Compact bone should have a large positive value near +1000 or more. In this manner, an acceptable gray scale will be established for the various anatomical substances. By using the Hounsfield number, the difference between attenuation coefficients of various body tissues is "amplified". For non medical applications more specific numbers can be defined.
The CT-number linearity is determined by plotting the CT-numbers for known materials versus their effective linear attenuation coefficients. The linear regression fit to the data should have a correlation coefficient of greater than 0.99.
10b. Spatial resolution
One of the performance criteria of CT scanners is their ability to image small objects; the ability of the scanner to image small objects depends upon its "spatial resolution". This parameter is correlated to the X-ray beam size, which is depending a sua volta on the beam collimation (see Section 6a) at the object position,on the detector size or collimation, on the translation and rotation steps,and on reconstruction algorithms.
Modern medical CT-scanners are capable of spatial resolution of 0.5 to 1 mm, and this parameter can be measured by a lucite slab having holes of varied sizes drilled into. Hole sizes range from 0.4 to 1.75 mm.
CT-scanners have the best spatial resolution with high subject contrast resolution (see Section 9c) like with the sample of plexiglas-air. The CT-scanner must also be able to image small objects with low contrast resolution. The difference between normal tissue and pathology is usually a small difference in CS.

In order to test low-contrast resolution, CT-scans are taken through a section in the phantom composed of a plastic with CT numbers only slightly different from water. This section contains various size holes that are filled with water.

10c.Contrast resolution

One of the most important parameter of computed tomography is the "contrast resolution" which can be defined as the ability of the CT-scanner to reveal differences in the transmission of X rays through an object containing structures which differ only slightly.

The contrast resolution depends at first on the difference in the attenuation coefficients of the different structures,which,on the other hand, depends on the energy of the incident monoenergetic X rays (Figure 38) or on the distribution of X-rays if bremsstrahlung radiation is employed.

For improving the contrast resolution between two structures of an object,the difference in the attenuation coefficient should be improved of the two structures,which mainly depends on the photoelectric and on the Compton effects. The Compton effect varies slightly with energy for elements or materials with contiguous atomic numbers, where the first one is critically dependent on the atomic number of the two structures. Then,almost theoretically, the contrast resolution will be improved by reducing the energy of the incident photon beam. On the other hand,reducing the energy of the beam, the absolute value of the attenuation coefficient also strongly increases, and the useful dimension of the object to be scanned should be reduced,according to the rule (see Eq. 29):

$$\mu \, x \, \simeq \, 1 \div 6$$

That rule limits the usefulness of using low energy radiation to non medical images or medical "in vitro" images,where scanning time and absorbed doses are not a problem.

From a general point of view, the contrast resolution is connected to:

-spatial resolution,influencing the number of voxels,as observed in Section 9a

-source intensity ($N_\circ$ photons/s), and incident energy $E_\circ$

-total run-time T(in s)

-number of translations and rotations N; $N \times N$ represents the number of voxels.

It can be demonstrated that,defining $\Delta\mu / \mu$ as the contrast resolution in terms of relative accuracy of the measured attenuation coefficients;

$$\Delta\mu/\mu = \frac{1.2 \ N^{5/2}}{\sqrt{T} \ \sqrt{N_\circ}} \tag{32}$$

when the condition given by Eq.(27) is valid.

By defining $N_{h,h}$ as the total number of photons emitted by the source during a tomography,then:

$$\Delta\mu/\mu = \frac{1.2 \ N^{5/2}}{\sqrt{N_{tot}}} \tag{33}$$

For a given value of the contrast,the number of projections and the total number of photons emitted by the source are connected together. If the photon flux is decreased,the same contrast can be achieved only by reducing the number of voxels.

Curves showing Eq.(33) are depicted in Figure 39.

A contrast scale CS can also be defined, as the change in the effective attenuation coefficient per CT number unit. Usually,measurements are performed with reference to plexiglas and water, and the contrast scale is represented by the following equation:

$$CS = \frac{\mu_{plex} - \mu_w}{(CT)_{plex} - (CT)_w} \tag{34}$$

10d.Image noise

When one images a uniform material in a CT scanner, the CT numbers for a localized region should be the same. In practice the CT numbers vary around some average value. The reasons for these variations can be:

-statistics of the countings

-changes in the source (mainly changes in X-ray units)

-drifts in the detectors

-electronic noise

-small errors in the algorithms.

All of these parameters introduce variations in the CT numbers. The variations are lumped collectively into a term called the noise of the CT-system.

The noise can be experimentally determined by scanning a uniform water sample and evaluating the different CT numbers in a small region. The mean value (X) and the standard deviation (σ) of the CT numbers are computed. The CT noise is then expressed as a percentage variation of the linear attenuation coefficient:

$$\%\,\sigma_w = \frac{100 \ \sigma \ CS}{\mu_w} \tag{35}$$

The noise values for CT-scanners are important performance parameters.The difference in the attenuation coefficients between normal and pathological tissues is small. High CT noise values tend to obscure small tissue difference.

The CT noise levels,however, are a function of many parameters. For medical imaging,noise levels decrease as the radiation dose increases and as the slice thickness increases. The noise levels

are also higher for large patients. The relationship of the various factors to the noise level is usually given as the following Equation:

$$\sigma_N = \sqrt{\dfrac{B}{H\,D\,W^3}} \qquad (36)$$

where B is percentage attenuation, H is slice thickness, W is pixel width size and d is patient dose per scan.

10e. Distortion and artifacts
Artifacts are significant problems in CT imaging. They come from a variety of sources. Typical artifacts sources include:
-patient motion (in medical images)
-high-attenuation objects (in industrial images)
-aliasing (higher-frequency information appears as artifactual information at lower frequencies
-beam hardening (by using non-monoenergetic radiation)
-detector imbalance (rings),when more detectors are used
-centering
-partial volume effects

10f. Absorbed dose
In medical CT imaging, the radiation dose delivered to a patient during a CT examination varies from unit to unit and also over the section of tissue exposed. The absorbed dose delivered by a CT unit can be described by dose profiles obtained at various depths in a phantom. In Figure 40 are shown dose profiles at the surface and at midline for single section examination of a patient.
The absorbed dose delivered during a CT procedure depends primarly on the level of noise that can be tolerated in the image and on the efficiency with which the transmitted photons are utilized by the detectors.

11. Trends in X-ray imaging
11a. Differential tomography
Photoelectric attenuation coefficient (see also Section 3a) and therefore attenuation coefficient of every element exhibits sharp discontinuities (K,L,......) in correspondence with the minimum energy values for the ejection of the electron from its shell (Figure 41). For quantitative evaluation,values of attenuation coefficients of Fe, Ag, I and Pb near K and L-edges are shown in Table 8 . As can be observed,the difference in the attenuation coefficient and above and below the edges is large. When two attenuation measurements are carried out with a pair of monoenergetic radiation beam whose energies bracket the discontinuity, then the difference between the two measurements is sensitive only to the presence of the element. This effect has been known for a long time in radiology for the visualization of

iodinated vessels (energy-dependent subtraction angiography). In this case, bremsstrahlung radiation was employed generated at different HV-values of the X-ray tube,instead of monoenergetic radiation.
Let us consider,as an example,a matrix of thickness x containing an element a at concentration c_a . If we use a beam of X-rays made up of two energies E_1 and E_2 ,which bracket the photoelectric edge of the element a, the attenuation is given by:

$$N_1 = N_{10}\; exp\left\{ \left[\mu_{m1}(1-c_a)+\mu_{a1}\,c_a \right] x \right\}$$

$$N_2 = N_{20}\; exp\left\{ \left[\mu_{m2}(1-c_a)+\mu_{a2}\,c_a \right] x \right\} \qquad (37)$$

In Eqs.(37), N_{o1} , N_{o2} , N_1 and N_2 represent the intensity of incident and transmitted radiation of energies E_1 and E_2 respectively, μ_{m1} , μ_{m2} , μ_{a1} and μ_{a2} represent the attenuation coefficients of the matrix and of the element a at energies E_1 and E_2 respectively. The ratio N_2/N_1 can be written as:

$$R = R_o\; exp - \left[\left(\Delta\mu_m - c_a(\Delta\mu_m - \Delta\mu_a) \right) x \right] \qquad (38)$$

where $R_0 = N_{20}/N_{10}$, $\Delta\mu_m = (\mu_{m2}-\mu_{m1})$; $\Delta\mu_a = (\mu_{a1}-\mu_{a2})$
Close to the edge is further valid the condition $\Delta\mu_m \ll \Delta\mu_a$. Then:

$$R = R_o\; exp\left[\Delta\mu_a\, c_a\, x \right] \qquad (39)$$

The differential transmission and the differential tomography are therefore only depending,at a first approximation, on the concentration c_a of the element to be analyzed. It can be calculated that the sensitivity of the method ranges between 300-400 ppm,for medium atomic number elements.
Differential tomographic images have been carried out at energies above and below the K-discontinuity of silver and iodine (30).For silver,which has the K-discontinuity at 25.517 keV, secondary targets of tin (K_a =25.15 keV) and antimony (K_a =26.2 keV) have been employed. Results carried out on a plexiglas cylinder with two holes filled with Ag solutions are shown in Figure 42. For iodine, which has the K-discontinuity at 33.164 keV, various pairs have been examined: Ba-K_a and Kβ (32 and 36.4 keV respectively) Ba-K_a and Ce-K_a (32 keV and 34.5 keV respectively) and La-K_{a1} and K_{a2} (33.033 keV and 33.44 keV respectively). Images are better for closer energy pair,because of the matrix effect neglected in Eq. (39). Images obtained by using the La-pair are shown in Figure 43.
The same principle was employed by Fryar et al.(31).These authors employed a 3 mCi Cd-109 source emitting silver X-rays (22 keV and 25.2 keV) for imaging palladium (K-edge at 24.4 keV).
The same authors also used secondary X-rays emitted from barium

excited by an Am-241 source for detection cesium, and an X-ray tube with external filters for selective images of palladium,silver and cadmium (Figure 44).
The sensitivity of differential CT-images is a function of atomic number of the element to be detected; in the best conditions it is about 200 ppm (31).

11b. XRF-tomography
Fluorescent X-ray tomography (XRF-tomography) is based on the detection of the fluorescent X-rays emitted by a single voxel in an irradiated sample (32).The principle of the method is shown in Figure 45). The output of the X-ray tube is strongly collimated by a collimator 6 cm long and diameter of 0.5-1 mm, which delimits the object to be scanned as a section of a conical volume. The detector, which analyzes the X-rays emitted from the irradiated volume, is also strongly collimated in the same manner as the source, and is placed at 90 degrees with respect to the primary radiation, thus delimiting the analyzed voxel as the intersection of incident and output radiation. By moving the object in the x-y plane, X-ray intensity of elements present in the sample which X-rays are collected and analyzed, can be mapped, and finally an image can be obtained related to the distribution of the elements in the sample.
As an example,let us consider a sample containing an element a at concentration c_a ,irradiated with N_o photons of energy E_o in a 90 degrees geometry.
Deviding the section of the sample into many voxels in which the attenuation of both incident and output radiation can be neglected,so that each voxel can be considered like a thin sample, X-rays N_a emitted by element a are given by:

$$N_a = N_o k \omega_a \mu_{ph,a}(E_o) \, 0.7 \, m \, c_a \qquad (40)$$

where the parameters have the following meaning:
- K is an overall geometrical efficiency
- ω_a is the fluorescence yield of element a
- $\mu_{ph,a}$ is the photoelectric attenuation coefficient of element a at incident energy E_o
- m is the mass per unit area of the sample.
There is a linear relationship between the concentration c_a and the number of X-rays of element a, N_a ,emitted by the considered voxel.
It should be observed that the irradiated volume varies with the distance between the sample to both the source and the detector;by moving only the sample in the x-y plane the irradiated volume may be kept constant.
Calling m the voxel number in the y-axis, n in the x-axis,each voxel can be identified by an mn index. X-ray counts of element a have to be corrected for attenuation effects,both of incident and

output radiation from the irradiated voxel.Counts in the detector related to the mn voxel are then given by:

$$N_{mn} = N_a \, exp\left[\sum_{h=1}^{m-1} \mu_{hn} \, \Delta x\right] \cdot \left[\sum_{h'=n}^{x-1} \mu_{mh'} \, \Delta x\right] \qquad (41)$$

in which N_a is given by Eq.(40).
A test object has been first analyzed,constituted by a plexiglas matrix 20 x 20 mm section, with 64 cylindrical holes of diameter ϕ =2 mm. The holes are empty,except those at the diagonal of the object,which are filled with a solution containing 0.5% iodine (Figure 46).
Other measurements have been carried out on LiF crystals,in order to study the migration of silver ions into the crystal after heating (Figure 47). All these measurements have been performed using the direct bremsstrahlung output of an X-ray tube, because of the very strong collimation of primary and secondary radiation.
Bavdaz et al.(33) used synchrotron radiation as a more collimated,high intensity source to map elements in a low Z matrix. The advantages of using synchrotron radiation instead of X-ray tubes lies mainly in the high photon and monochromatic flux, the negative point in the fact that high photon fluxes are usually available at energies untill about 15-20 keV.
Very small objects were scanned (0.5 mm) with a very high spatial resolution (about 5 μm). An image of nickel grains in a polymer matrix is shown in Figure 48 .

11c. Microtomography
High resolution X-ray imaging (microtomography) may be defined as the process of recording transmitted X-ray beams which are spatially modulated by the material under study, with resolution of 10 m or less. Low to medium energy X-rays are typically used in order to maintain high contrast and resolution. Until recently, most applications of microtomography have involved biological specimens, but there is no intrinsic reason for this limited applications, and material analysis applications are now appearing. The availability of microtomography scanners with penetrating radiation will clearly have a significant impact on material science.

Cruvinel for cooperation and useful discussions.
We wish also to acknowledge Prof. G.E. Gigante and Dr. E.
Staderini for useful discussions.

13. References

1)R. Cesareo, Photon induced X-ray emission, in R. Cesareo Ed.,
Nuclear analytical Techniques in Medicine, Elsevier,Amsterdam,
Oxford, New York, 1988,pp.19-119.

2)J.H. Hubbell, Wm.J. Veigele,E.A.Briggs,R.T.Brown, D.T. Cromer
and R.J. Howerton, J. Phys. Chem. Ref. Data 4(1975) 307.

3)R.D. Evans, in Flugge (Ed.), Encyclopedia of Physics, Vol.
XXXIV,Springer Verlag, Berlin,Gottingen,Heidelberg,(1958)
pp.218-298.

4)J.H. Hubbell,Photon cross sections,attenuation coefficients and
energy absorption coefficients from 10 keV to 100 GeV, NSRDS-NBS
29,1969.

5)E.C. McCullough, Med. Phys. 6(1975)307.

6)G.R.Hammerstein,D.W.Miller,D.R.White,M.E.Masterson,H.Q.Woodhard
and J.S.Laughlin, Radiology 130 (1979) 485.

7)P.C.Johns and M.J.Yaffe, Phys.Med.Biol. 32 (1987) 675.

8)ICRP, Rep. on the task group on reference man, Rep. 23, Oxford
Pergamon

9)M.E.Phelps,E.J.Hoffman and M.M. Ter-Pogossian, Radiology 117
(1975) 573

10)P.S.Rao and E.C.Gregg, Am. J. Roentgenol. 123 (1975) 631.

11) J.Radon, Uber die Bestimmung von Funktionen durch ihre
integralwerte langst gewisser Mannigfaltigkeiten, Sachsische
Akademie der Wissenschaft, Leipzig 69 (1917) 262.

12)A.M.Cormack,Nobel Award addresses,Med.Phys.7 (1980)277.

13)A.M.Cormack,J.Appl.Physics,34 (1963)2722

14)A.M.Cormack,J.Appl. Physics,35 (1964) 2908.

15)O.J.Tretiak, M.Eden, W.Simon, Internal structure from X-ray
images,Proc. eighth Int. Conf. on Med. and biol. Engineering,
IEEE, Chicago 1969.

16)R.H.T. Bates and T.M. Peters, Towards improvements in
tomography, N.Z.J.Sci. 14 (1971) 883.

17)G.N.Hounsfield,Nobel Award Addresses,Med.Phys. 7(1980) 283.

18)R. Cesareo,L.J. Pedraza, Nucl. Instrum. Methods in Phys. Res.
A239 (1985) 367.

19)J.S.Iwanczyk,A.J.Dabrowski,G.C.Huth,J.G.Bradley,J.M.Conley,A.L.
Alber,IEEE Trans. Nucl. Sci. 33(1986) 355.

20)N.McCuaig,A.A. Tajuddin,W.B. Gilboy,J.W. Leake, Nucl. Instrum.
Methods in Phys. Res. A242 (1986) 620.

21)The Radiochemical Centre, Amersham; Radiation sources 1989-90.

22)J.T. Merrifield,Aviation Week,march 1986,vol.124 n.9,81.

23)S.Crestana,R.Cesareo,S.Mascarenhas,Soil Sci. 142 (1986) 56.

24)R.Cesareo, Nucl. Instrum. Methods in Phys. Res. A275
(1989)420.

25)P. Burnstein,P.J.Bjorkholm,R.C. Chase, F.H. Seguin, Nucl.
Instrum. Methods in Phys. Res. 221(1984) 207.

26)P.Reimers,J.Goebbels,H.P.Weise,K.Wilding, Nucl.Instrum.
Methods in Phys. Res. 221(1984) 201.

27)R. Cesareo, Cracow Conference on non-destructive testing,
Cracow (Poland) 1990.

28)K. Tsumaki,T.Kanamori,F.Takahashi,T.Ikeda,Nucl. Sci. and
Technol. 214 (1984) 315.

29)B.D. Sawicka and R.L. Tapping, Nucl. Instrum. Methods in Phys.
Res. A256 (1987) 103.

30)R. Cesareo, Nucl. Instrum. Methods in Phys. Res. A270 (1988)
572.

31)J. Fryar, K.J. McCarthy, A. Fenelon, Nucl. Instrum. Methods in
Phys. Res. A271 (1988) 571.

32)R. Cesareo, S. Mascarenhas, Nuclear Instrum. Methods in Phys.
Res. A277 (1989) 669.

33)M. Bavdaz, A. Knochel, P. Ketelson,W. Petersen, N. Gurker,
Nucl. Instrum. Methods in Phys. Res. A 266 (1988)308.

Table 1 – Electron density δ_e of various elements, compounds and mixtures

Element	atomic number Z or formula	electron density (el/cm³)
hydrogen	1	6 x 10
carbon	6	3 x 10
nitrogen	7	3.01 x 10
sulphur	16	2.89 "
potassium	19	2.93 "
chromium	24	2.78 "
iron	26	2.80 "
zinc	30	2.76 "
arsenic	33	2.65 "
silver	47	2.63 "
iodine	53	2.51 "
lead	82	2.38 "
Compounds or mixtures		
muscle	–	3.47 "
blood	–	3.48 "
fat	–	3.15 "
polyethylene	(CH)	3.17 "
water	H O	3.35 "
nylon	–	3.8 "
lucite	(C H O)	3.87 "
bakelite	(C H O)	4.27 "
teflon	–	6.33 "

Table 2 – Total electron cross section (cm²/electron) versus atomic number Z, at 10,60 and 200 keV

element	atomic number Z	10 keV	60 keV	200 keV
oxygen	8	19.25	0.635	0.41
aluminum	13	91	0.96	0.42
sulfur	16	170	1.34	0.43
calcium	20	321	2.16	0.46
iron	26	615	4.31	0.52
copper	29	817	5.9	0.57
molybdenum	42		16.7	0.93
tin	50		25.8	1.29
iodine	53		31	1.48
tungsten	74		15.2	3.2
lead	82		20.4	4.15
uranium	92		30	5.5

Table 3 – Weight fractions w_i for biological materials

Tissue	H	C	N	O	Na	P	Cl	K
H O	0.112	–	–	0.888	–	–	–	–
air	–	–	0.755	0.332	–	–	–	–
bone	0.064	0.278	0.027	0.410	–	0.07	–	–
muscle	0.102	0.123	0.035	0.729	0.001	0.002	–	0.03
brain	0.104	0.161	0.039	0.684	0.002	0.003	–	0.003
heart	0.106	0.124	0.025	0.744	–	–	–	–
kidney	0.096	0.030	0.122	0.729	0.002	0.002	0.002	0.002
liver	0.11	0.041	0.012	0.825	–	–	0.012	–
lungs	0.105	0.095	0.025	0.766	–	0.007	–	–
pancreas	0.107	0.072	0.023	0.800	–	–	–	–
spleen	0.105	0.101	0.027	0.765	–	–	–	–

Table 4 – Photon attenuation coefficient of breast tissues versus energy

Tissue type	N. of patients	linear attenuation coefficient (cm⁻¹) at given energy in keV				
		20	30	50	80	110
fat	7	0.456	0.264	0.194	0.167	0.152
fibrous	8	0.802	0.378	0.233	0.189	0.170
carcinoma	6	0.844	0.392	0.238	0.192	0.173

Table 5 - Linear attenuation coefficients (in cm⁻¹) as a function of photon energy for various fluids and body tissues

Energy (keV)	Exp. values of linear attenuation coefficient (cm⁻¹)				
	blood	fat	muscle	pancreas	liver
17.7	1.159	0.665	1.153	1.142	1.175
21.1	0.762	0.461	0.759	0.755	0.753
26.4	0.489	0.327	0.485	0.484	0.493
27.4	0.460	0.317	0.455	0.454	0.46
31.1	0.378	0.276	0.375	0.375	0.377
35.5	0.319	0.245	0.318	0.317	0.322
41.4	0.274	0.219	0.274	0.274	0.277
47.2	0.246	0.204	0.248	0.247	0.25
52.0	0.237	0.195	0.233	0.232	0.233
59.6	0.221	0.184	0.213	0.216	0.217
84.3	0.191	0.166	0.189	0.189	0.19
97.4	0.178	0.161	0.180	0.179	0.182
121.9	0.169	0.152	0.168	0.167	0.168

Table 6 - Mean penetration (x , in μm) of radiation and scattering to photoelectric effects in copper and lead collimators versus energy

energy E	x		sc./phot.	
	copper	lead	copper	lead
10	3	4.6	0.007	0.04
20	20	7	0.022	0.03
40	150	44	0.072	0.07
60	500	125	0.17	0.13
100	1500	110	0.6	0.06
200		630		0.17
500		3800		0.9
1000		8600		2.8

Table 7 - Production of quasi monoenergetic X-rays by converting bremsstrahlung radiation into quasi monoenergetic lines with secondary targets. Efficiency of the conversion (scattering and photoelectric cross sections)

Target element	scattering cross section *	photoelectric	sc/ph
Cu	170	2.3 x 10	0.007
Mo	170	1.3 x 10	0.013
Sn	160	8.6 x 10	0.019
W	130	3.3 x 10	0.04
Pb	120	2.5 x 10	0.05

* at energies above the photoelectric discontinuity.

Table 8 - Attenuation coefficient (cm²/g) for copper, silver, iodine and lead close to the K-photoelectric discontinuity and to the L-discontinuity (for lead)

Element	Energy of the edge (keV)	μ_1	μ_2	$\Delta\mu$	F
Cu	8.98	28	285	257	215
Ag	25.52	9.7	52	42	1050
I	33.16	7.5	32.5	25	5000
Pb	13.04(L$_{III}$)	73	153	80	
	15.21(L$_{II}$)	112	143	30	
	15.87(L$_{I}$)	136	141	5	
	88.0 (K)	1.8	6.6	4.8	400

(*) The factor F is defined as $F = \Delta\mu_{\rightarrow}/(\Delta\mu_{\leftarrow} c_{\leftarrow})$
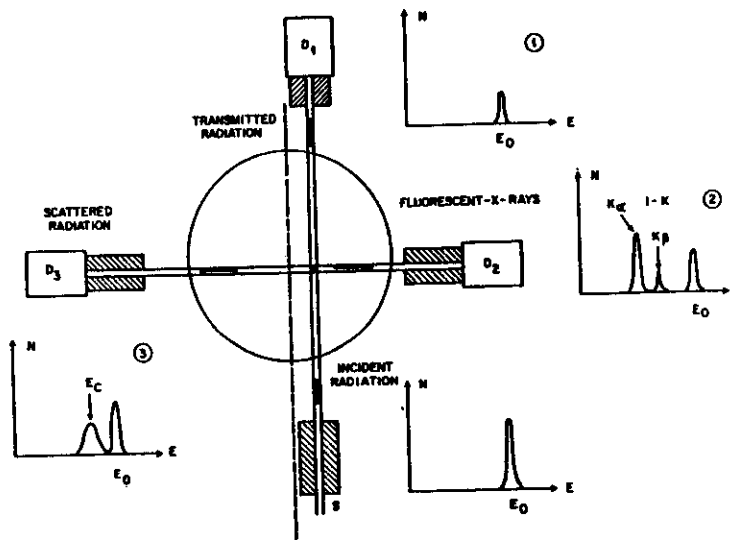
Figure 1 - When a sample is irradiated by a collimated beam of monoenergetic radiation,part of the radiation crosses the sample without be absorbed,and part is absorbed,giving rise to coherent and incoherent scattered radiation and to photoelectric effect with emission of secondary X-rays All these effects may be used for "imaging" the sample.
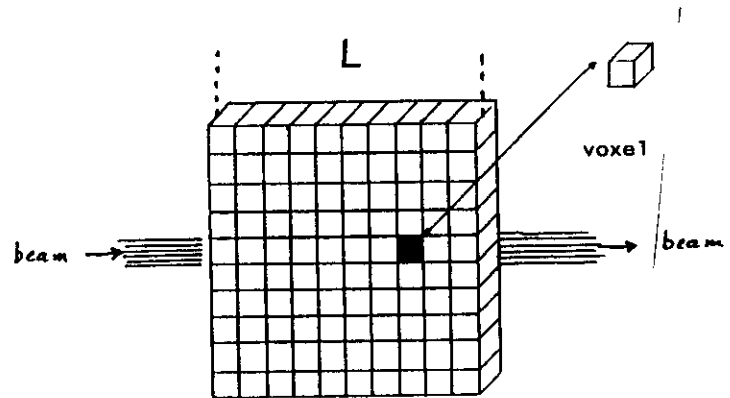
Figure 2 - Relation of the attenuation along the line L to the integral of the attenuation coefficient f along L. Definition of pixel.
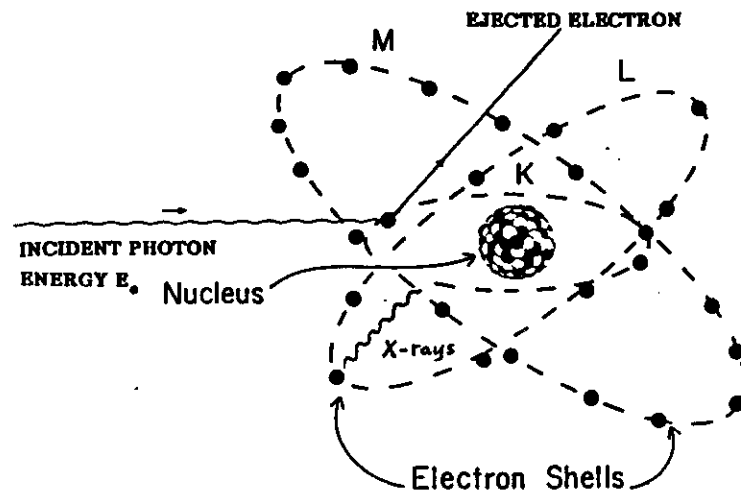
Figure 3 - Scheme for the photoelectric effect
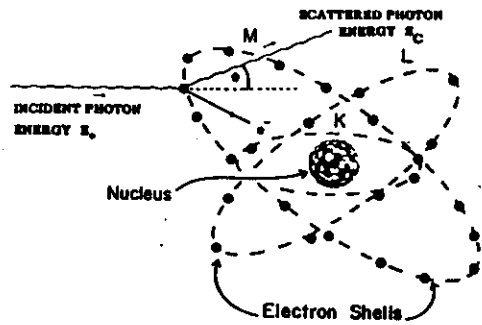
Figure 4 - Scheme for the Compton effect
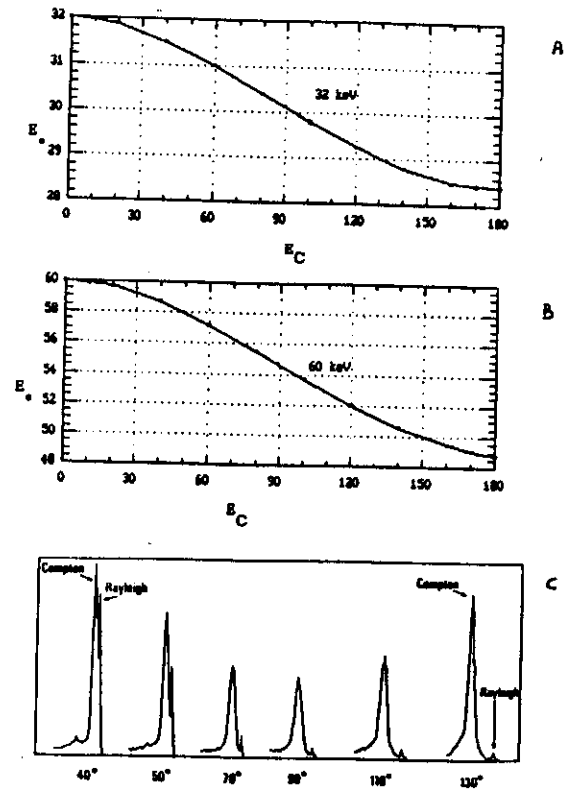
Figure 5 - Energy E_c of Compton scattered photons versus scattering angle ,for incident photons of 32 keV (A),and 60 keV (B).
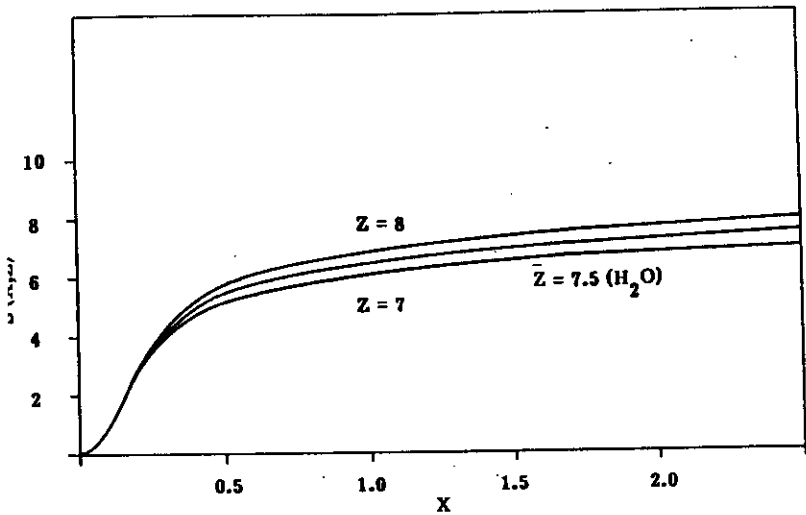
igure 6 - Incoherent scattering function $S(X,Z)$ for water versus momentum transfer X.
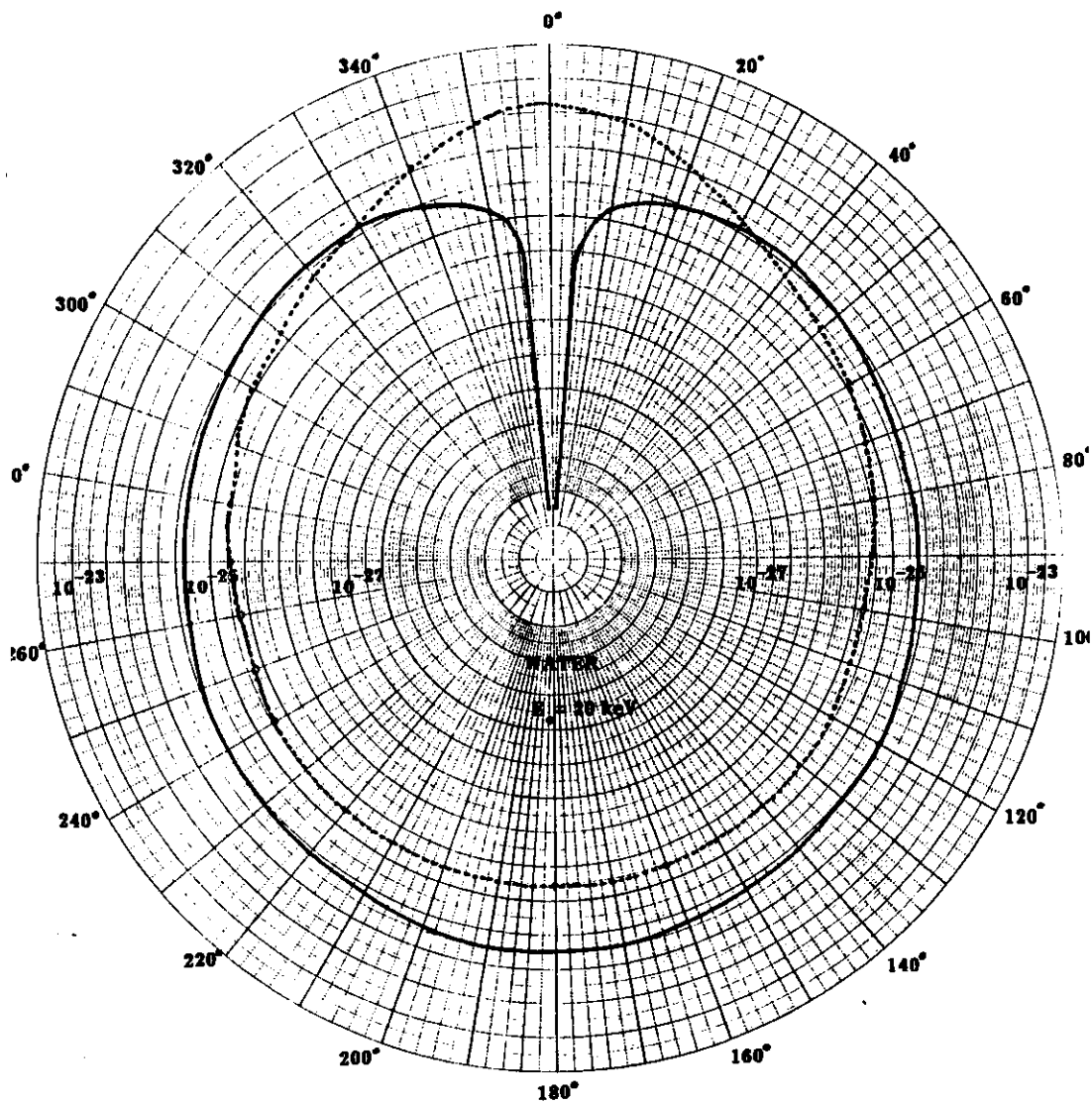
Figure 7 - Water differential cross section for Compton and Rayleigh scattering of 20 keV incident radiation.

Figure 8 – Water differential cross section for Compton and Rayleigh scattering at 40 keV incident energy.

46

Figure 9 – Silver differential cross section for Compton and Rayleigh scattering at 40 keV incident energy.

47
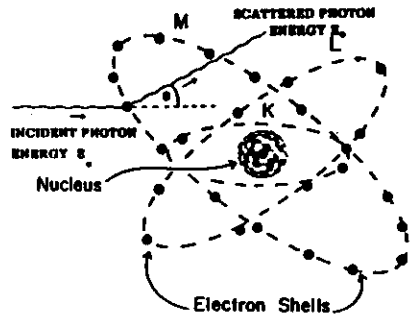
Figure 10 - Scheme for the coherent scattering
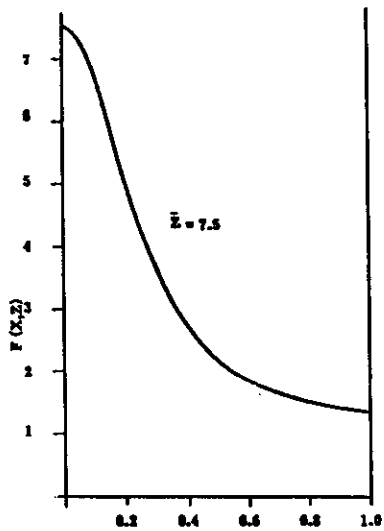
Figure 11 - Atomic form factor P(X,Z) for water and copper versus momentum transfer.
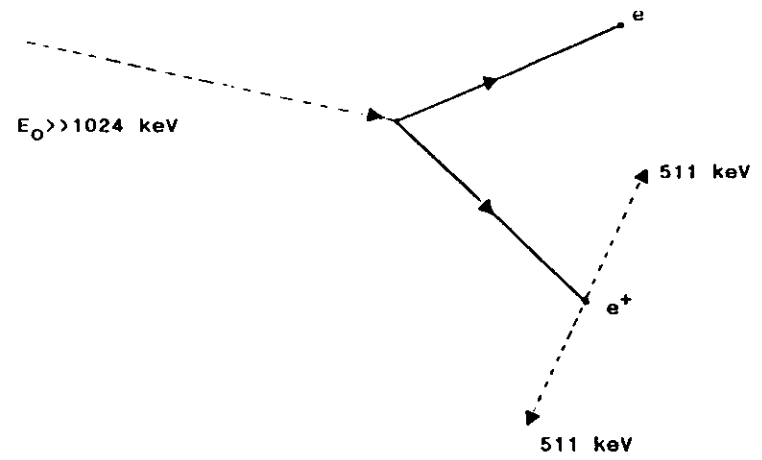
Figure 12 - Scheme for the pair production effect.
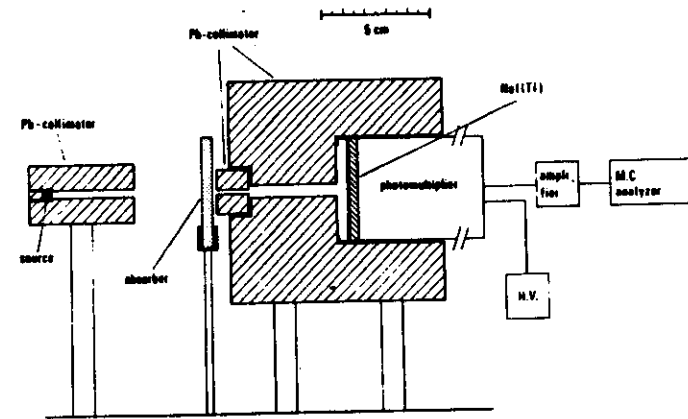
Figure 13 - Linear attenuation coefficient measurement in "good geometry".
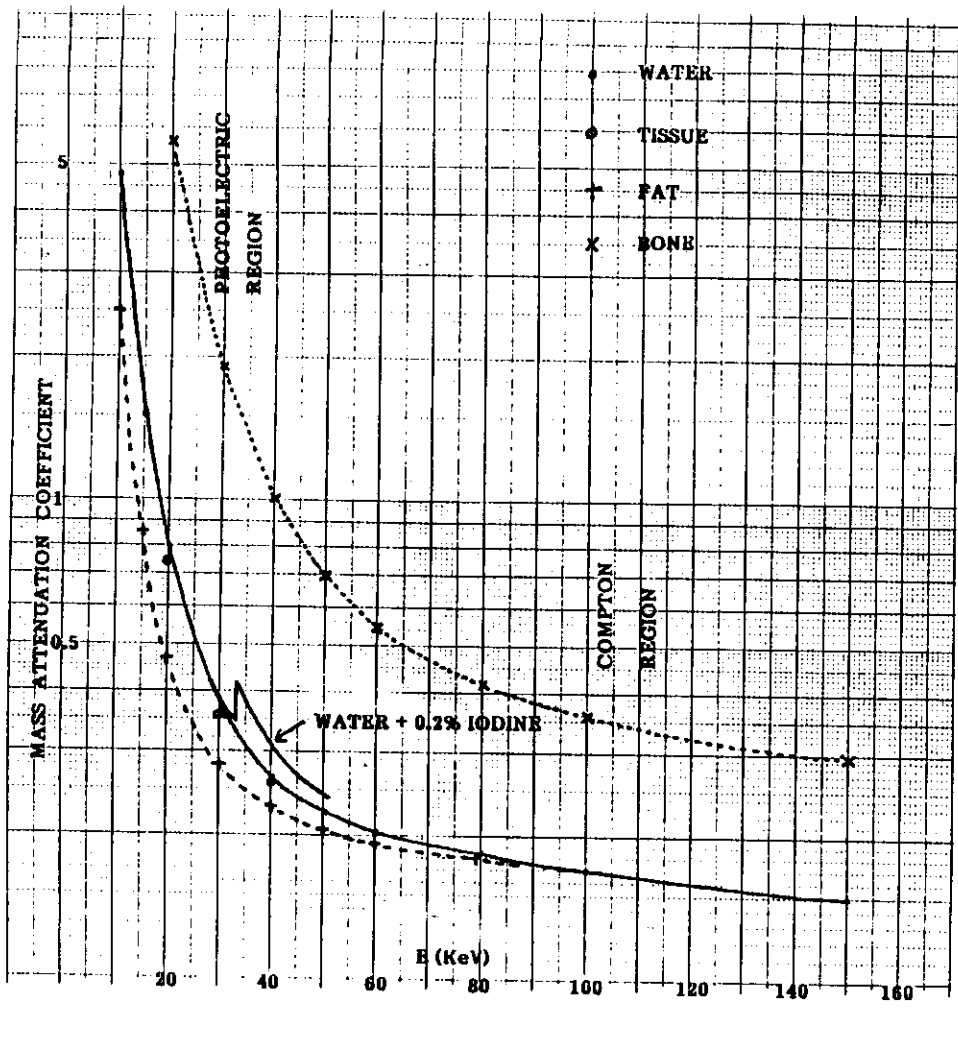
Figure 14 – Attenuation coefficient versus energy for some biological materials.
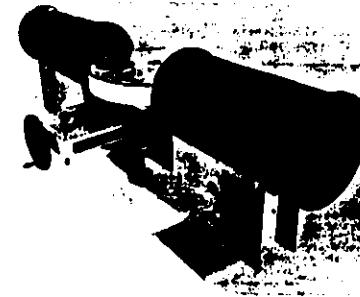
Figure 15 – Experimental apparatus used by Cormack in 1963 for measurement of attenuation coefficient of inhomogeneous samples.
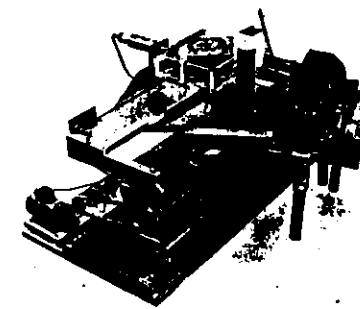
Figure 16 – Prototype of CT-scanner developed by Hounsfield in 1971.

Figure 17 - First CT-image of a brain,realized with the first prototype-scanner.
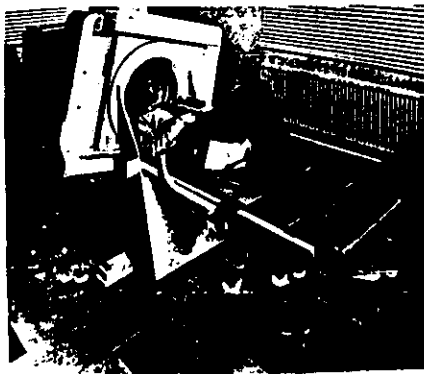
Figure 18 - First clinical CT-scanner installed at the A.Morley's hospital in Wimbledon.
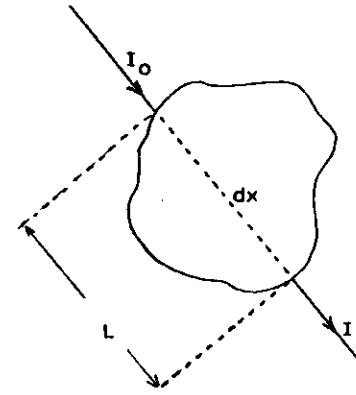
Figure 19 - Mathematical basis for computed tomography

SCAN 3

2.85 1.95 1.02

2.17

1.05

1	1.1	1.02
0.97	0.9	0.85
1.05	1.2	0.95

SCAN 1

$\rightarrow$ 3.12 $\rightarrow$

$\rightarrow$ 2.72 $\rightarrow$

$\rightarrow$ 3.2 $\rightarrow$

1.04	1.04	1.04
0.907	0.907	0.907
1.07	1.07	1.07

SCAN 2

3.02 3.2 2.82

3.017

1.011	1.1	0.974
0.908	0.968	0.841
1.071	1.13	1.001

0.974

1.942

3.013

2.039

1.071

0.987	1.105	1.02
0.973	0.914	0.845
1.05	1.196	0.95

Figure 20 - Iterative reconstruction method.

54

X-RAY TRANSMISSION

Y

X

X-RAY TRANSMISSION

Y

X

Figure 21 - Simple back-projection method.

55
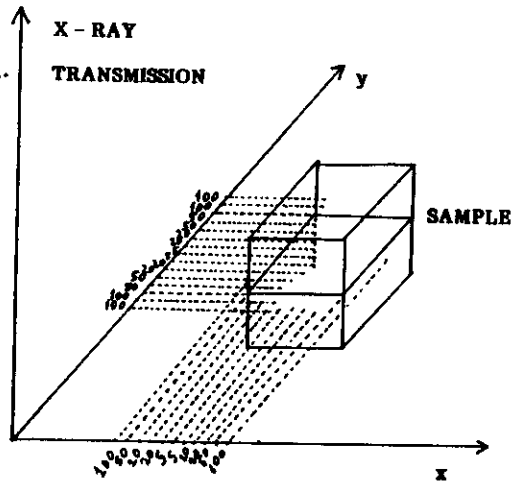
Figure 22 - Conceptional mathematics of simple back-projection.
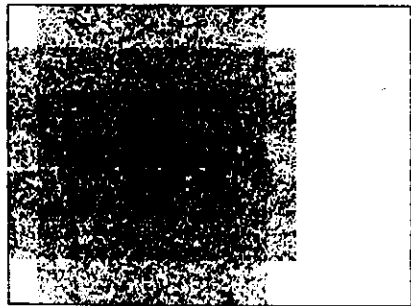
Figure 23 - Tomography relative to the scheme of fig.22 showing the simple back-projection concept.

56
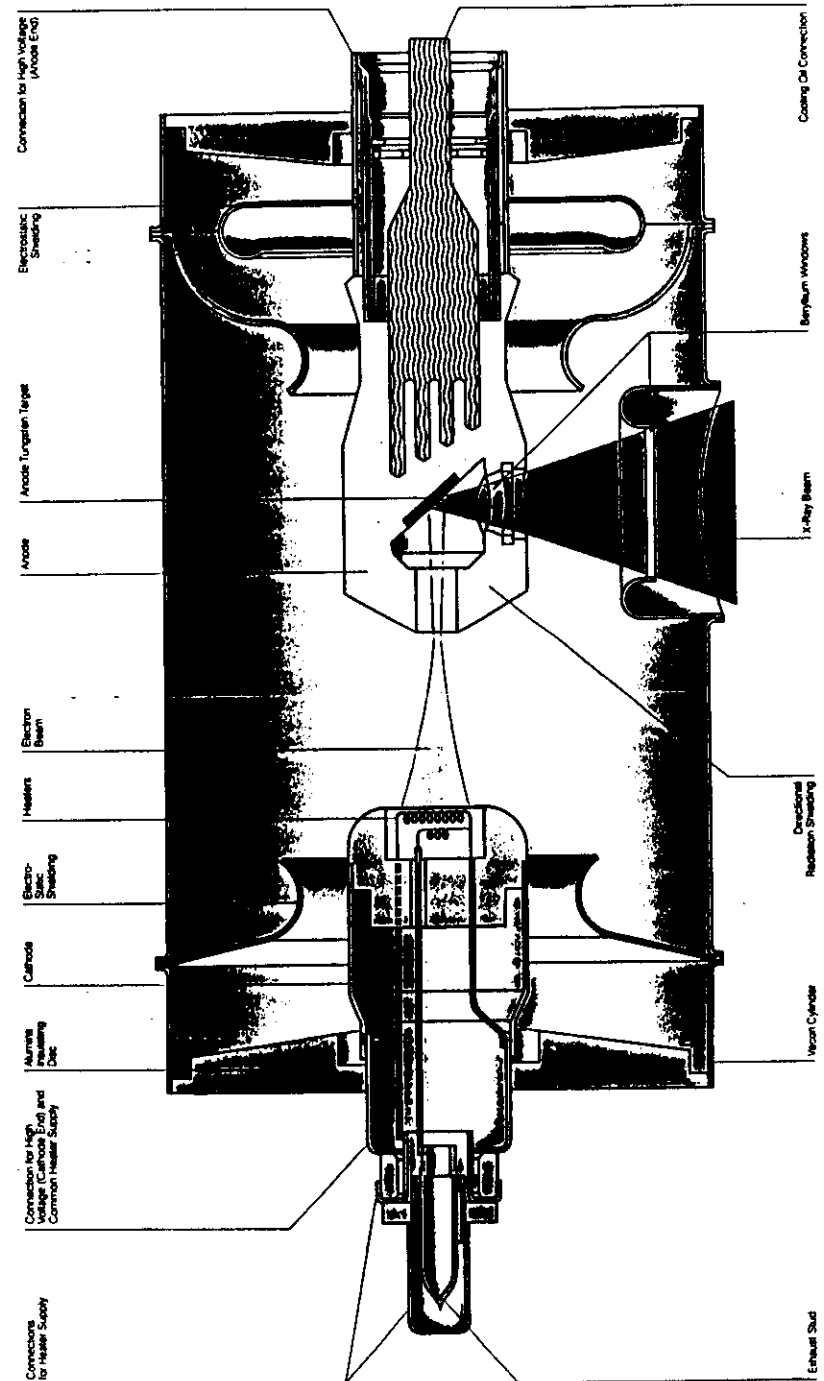
Figure 24 - Scheme of a typical X-ray tube

57
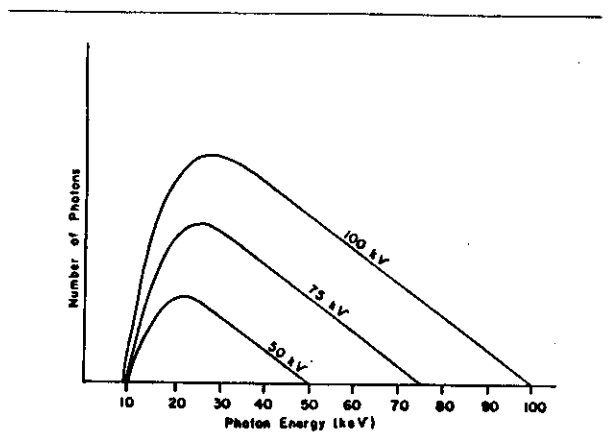
Figure 25 – X-ray spectrum of a typical tube versus kinetic energy of the electrons.
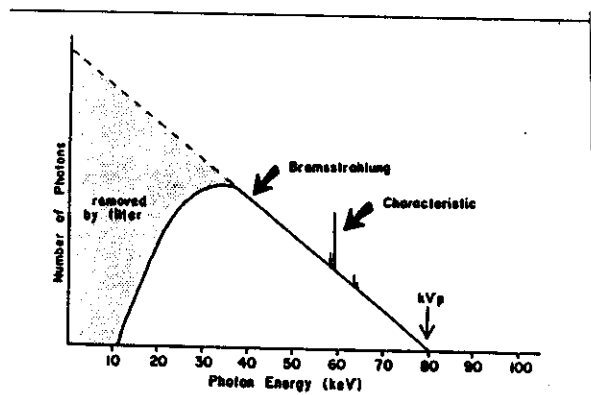
Figure 26 – Charactreristic X-rays from a W-anode of a X-ray tube
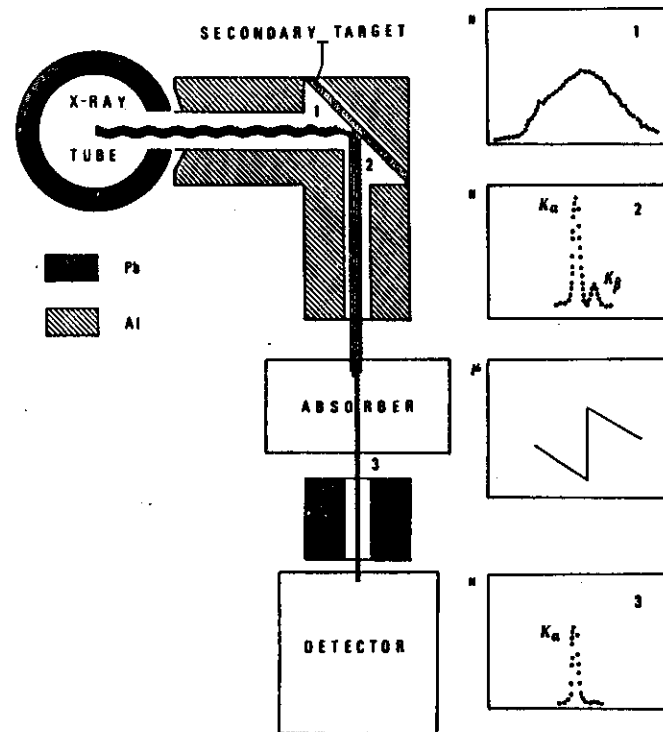
Figure 27 – Experimental set-up for the production of monoenergetic X-rays with a tube.

58

59
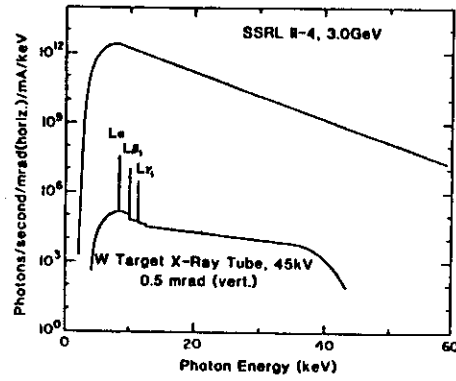
Figure 28 - Synchrotron radiation spectrum *from SPEAR at Stanford compared with a W-X-ray tube.*

Figure 30 - Output from a "hole" collimator

Figure 29 - Output from a cylindrical collimator
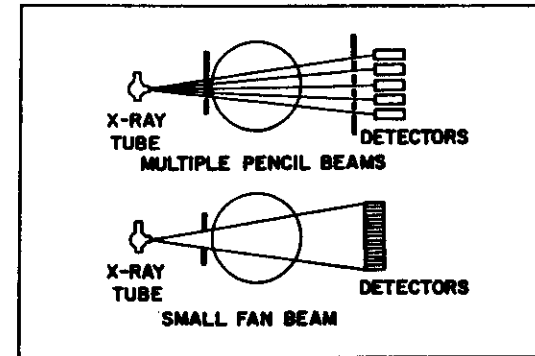
Figure 31 - Pencil-like X-ray beams and fan X-ray beams
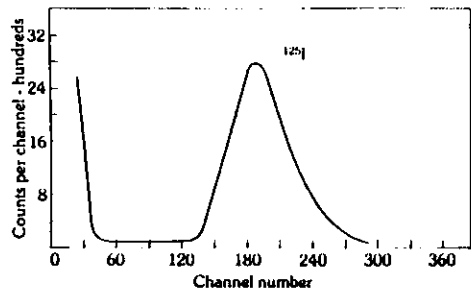
Figure 32 - Typical gamma spectrum of a CaF(Eu) detector
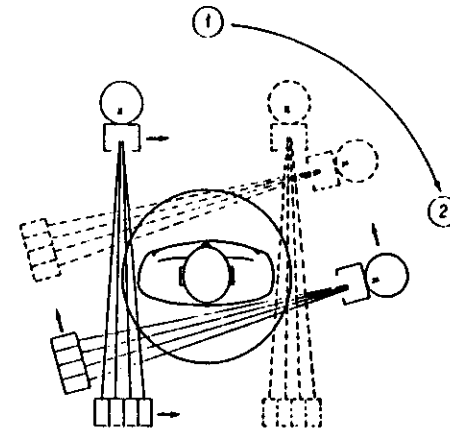
Figure 34 - Scheme of a first generation CT-scanner
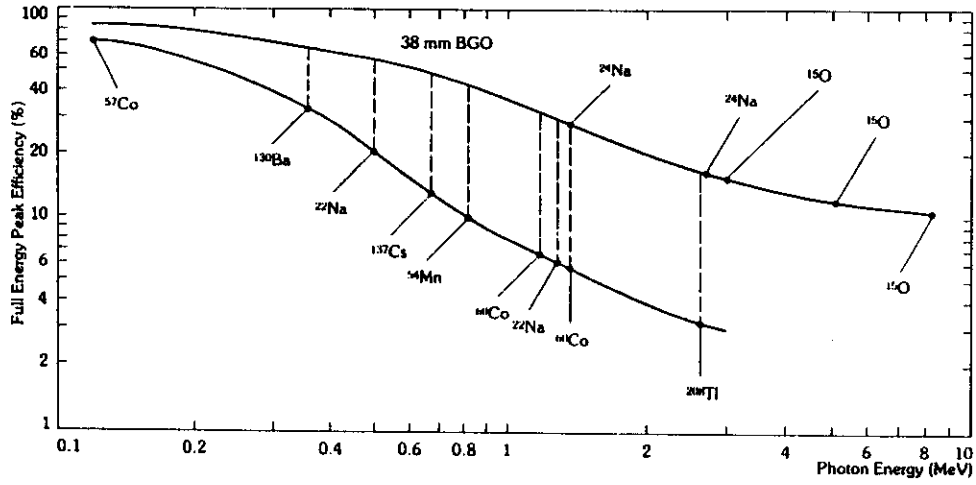
Figure 33 - Full energy peak efficiencies of a BGO and a NaI(Tl)
detector of 1 and 1/2" x 1 and 1/2".
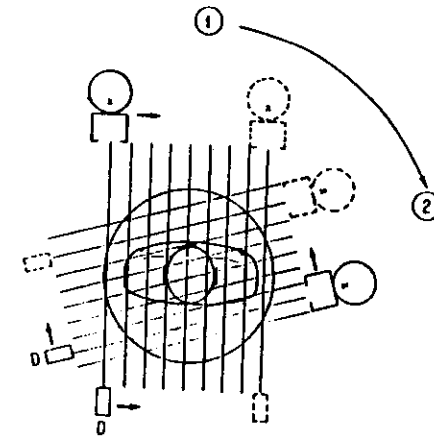
Figure 35 - Scheme of a second generation CT-scanner
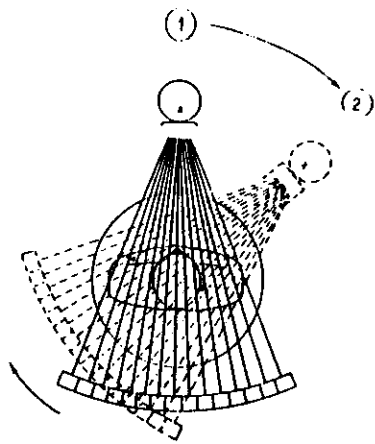
Figure 36 - Scheme of a third generation CT-scanner

Figure 37 - Scheme of a fourth generation CT-scanner

Figure 38 - Linear attenuation coefficient of structures of similar characteristics
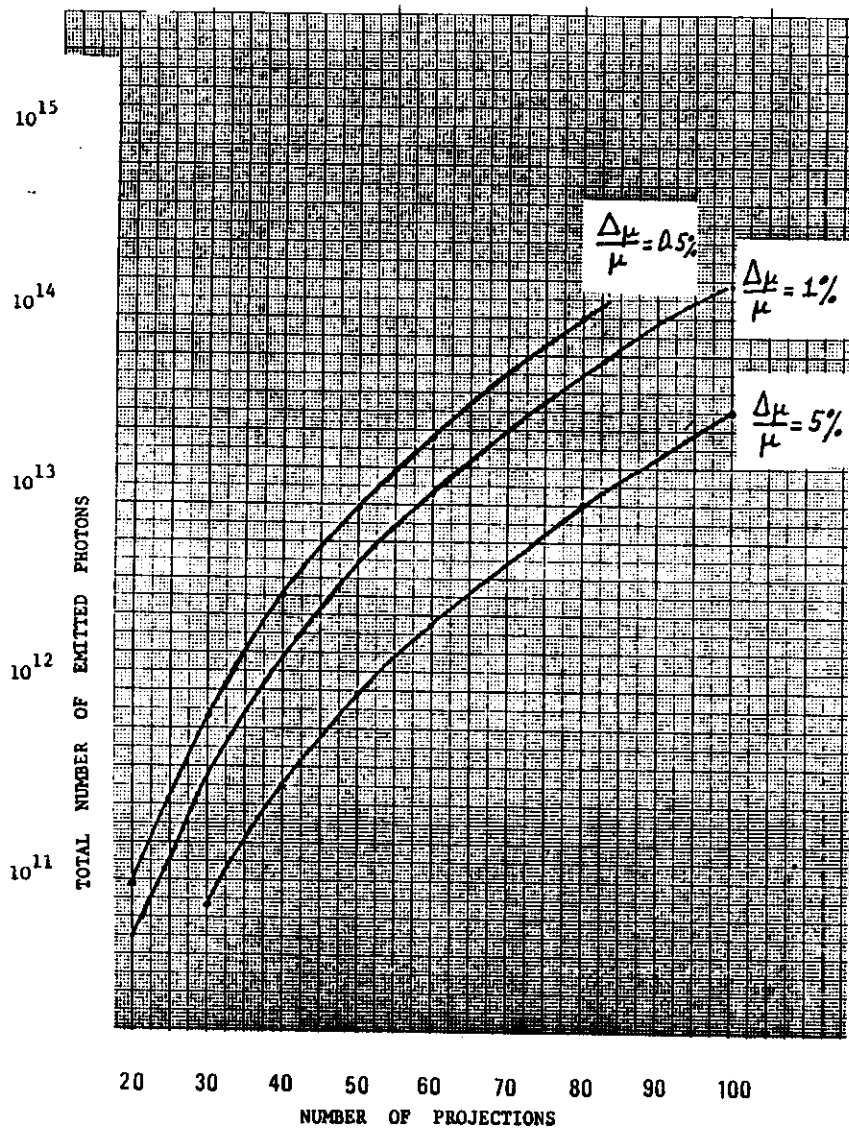
Figure 39 - Relative contrast resolution $\Delta\mu/\mu$ versus number of projections and total number of emitted photons
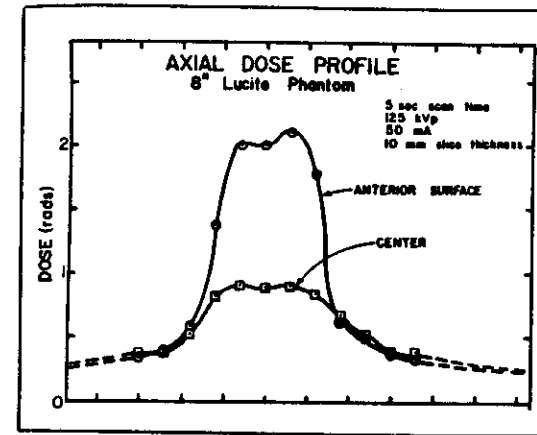
Figure 40 - Absorbed dose profiles at the surface of a patient examined with a fourth-generation CT-unit with 360 degree rotation of the X-ray tube
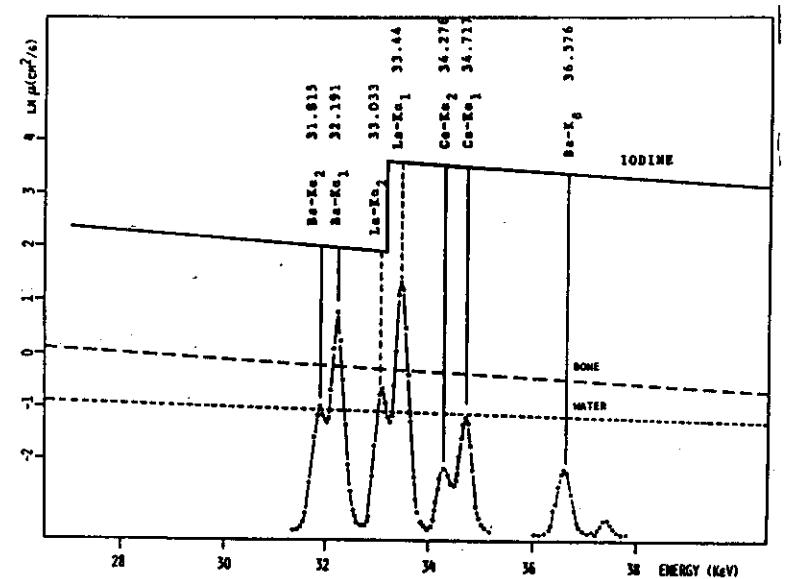
Figure 41 - Attenuation coefficient of iodine, showing the K-discontinuity and position of X-rays of barium, lanthanum and cerium, for differential tomographs of iodine.
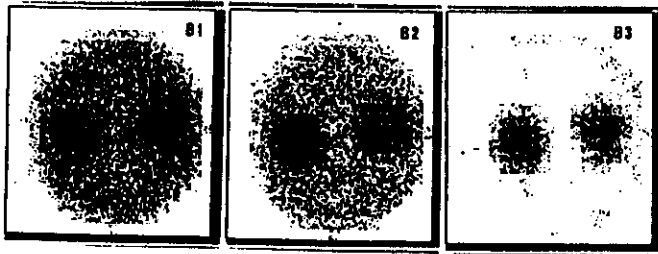
Figure 42 - Differential tomography of a plexiglas cylinder with two holes filled with 2% silver solution

Figure 43 - Differential tomography of a plexiglas cylinder with 4 holes containing iodine-solutions at 4,2,1,and 0.5% carried out with a lanthanum secondary target.
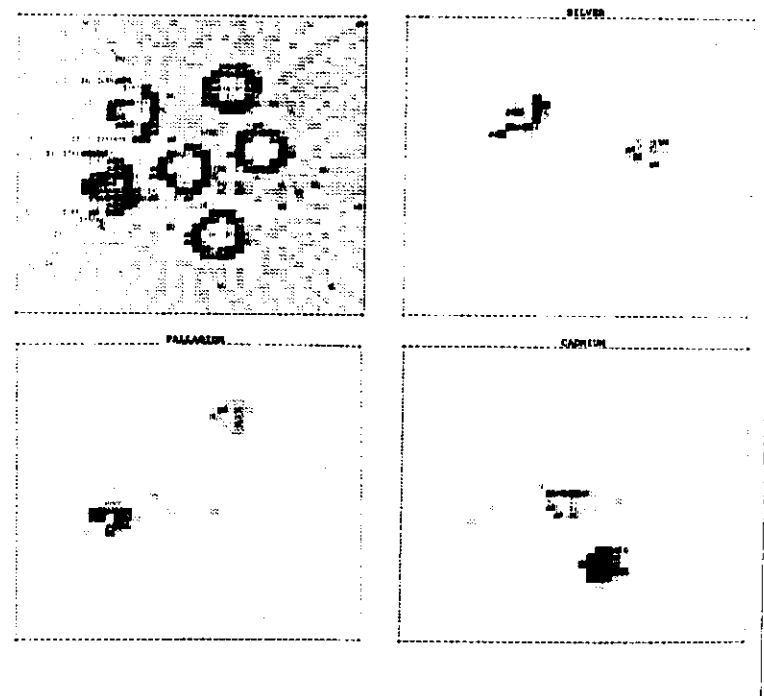
Figure 44 - A) Transmission tomography of a test object containing Pd, Ag and Cd grains.
B) Differential tomography of Pd
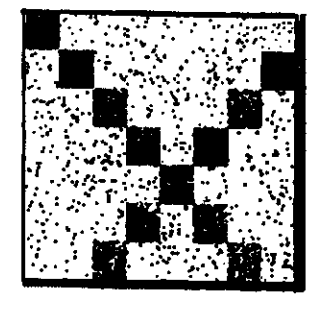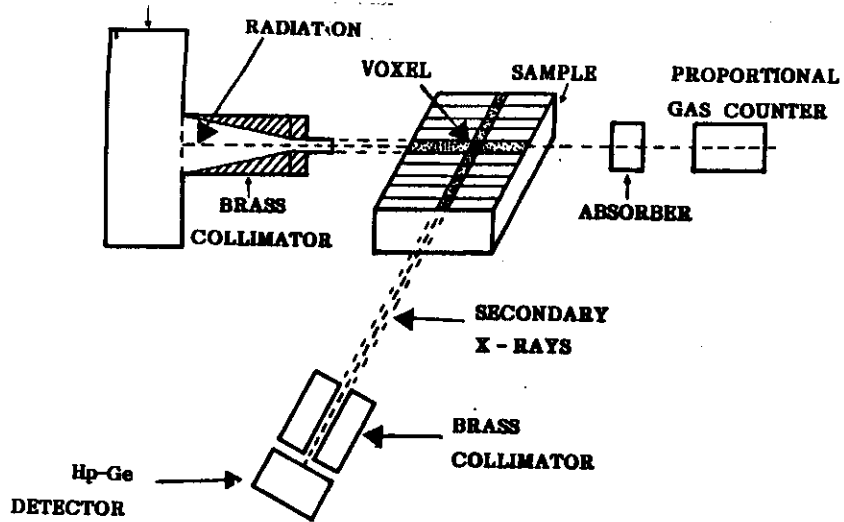C) Differential tomography of Ag
D) Differential tomography of Cd

Figure 46 - X-ray fluorescence tomography of a test object on plexiglas with holes at the diagonal, filled with a 0.5% iodine solution.
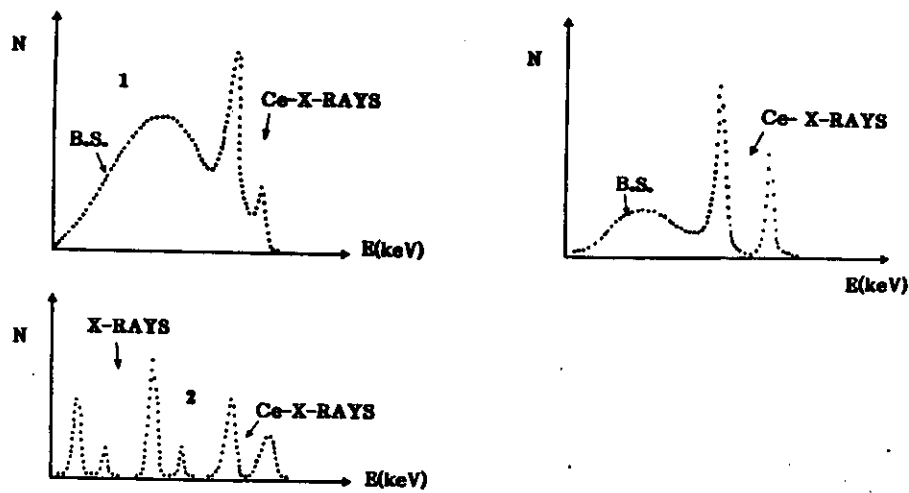
Figure 45 - Experimental set-up for fluorescent X-ray (XRF) tomography.The primary radiation is highly collimated (when iodine is analyzed the collimator is covered internally by a Ce-mixture) just as the collimator which collect the radiation emitted at 90 degrees by the sample.The intersection of colli-mated primary and fluorescent secondary radiation defines a volume element ("voxel").
Typical primary and secondary spectra are also shown (1 and 2) and transmitted spectrum (3).
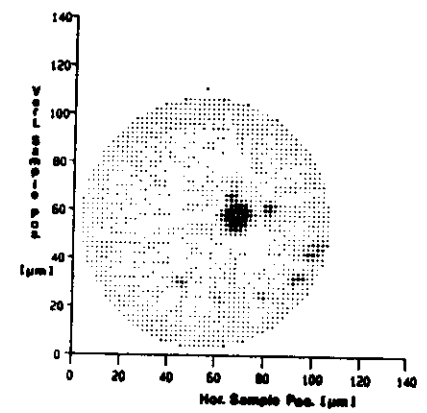

Figure 47 -Fluorescence X-ray tomography of nickel grains in an organic polymer matrix

70

71